J. Fluid Mech. (2004), *vol.* 505, *pp.* 23–57.
DOI: 10.1017/S0022112004008122 Printed in the United Kingdom

The theory of quasi-geostrophic von Kármán vortex streets in two-layer fluids on a beta-plane

By VLADIMIR M. GRYANIK[1,2], HARTMUT BORTH[1] AND DIRK OLBERS[1]

[1]Alfred-Wegener-Institute for Polar and Marine Research, Bremerhaven, Germany

[2]A. M. Obukhov Institute for Atmospheric Physics, Russian Academy of Sciences, Moscow, Russia

(Received 13 September 2001 and in revised form 12 November 2003)

In this study self-organized periodic coherent vortex structures arising in geophysical turbulent flows at low Rossby number are investigated by developing a conceptual model based on an analytical theory of von Kármán vortex streets affected by stratification and differential rotation. In the framework of a quasi-geostrophic (QG) two-layer beta-plane model vortex streets with three different types of vertical structures (barotropic, upper layer and hetonic) are analysed using the point vortex approximation. The streets are found to be exact solutions of the potential vorticity equation and to be characterized by four non-dimensional parameters. Von Kármán streets are semi-localized solutions which form a bridge between vortex pairs (limit of symmetric dilute streets) and two parallel vortex sheets (limit of dense streets). On the beta-plane QG von Kármán streets can only move to the east, i.e. with a speed outside the range of speeds of Rossby waves, so that a dynamical asymmetry in the zonal direction is introduced. A complete classification on a diagram of states shows that critical bounds exist in the parameter space, prescribing for example a maximum distance between vortex rows beyond which no QG vortex streets can be found. Typically a fast and a slow vortex street with different flow structures are found in the region of existence. As a function of distance between vortex rows baroclinic QG vortex streets show a characteristic non-monotonic speed behaviour at scales of the order of the baroclinic Rossby radius. A wide region of possible existence of QG von Kármán streets is found in atmospheric, oceanic and planetary conditions as well as in rotating tank experiments. The theory can be applied to describe the coherent part of turbulent baroclinic intermittent zonal jet-like and frontal flows and provides a scaling for such flows.

1. Introduction

1.1. *Von Kármán streets in geophysical flows*

The organization of flows into vortex streets of von Kármán type is a widespread phenomenon in hydrodynamics, observed on scales ranging from flows in small laboratory tanks to flows on giant planets. The structure of the flows of von Kármán type is remarkably similar in all circumstances and can be described by the simple schematic model shown in figure 1. Von Kármán vortex streets (Kármán 1911) are formed by two parallel rows of equally spaced vortices all having the same strength – with positive (cyclonic) vorticity in one row (solid circles) and negative (anticyclonic) in the other (open circles). In this model only three parameters are needed to characterize a street: the zonal distance a between vortices, the distance between rows b

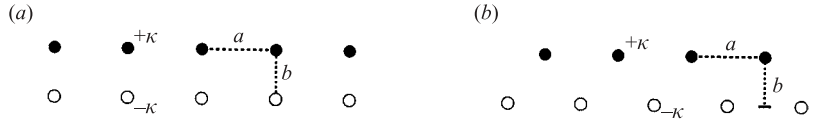

FIGURE 1. Horizontal structure of symmetric streets (a) and antisymmetric streets (b).

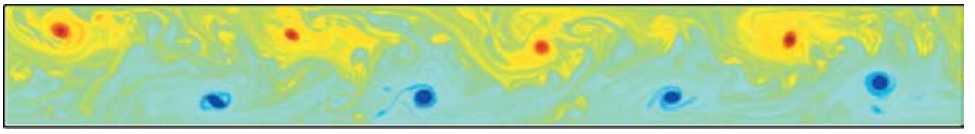

FIGURE 2. Self-organized westward propagating antisymmetric vortex street in a wind-driven turbulent two-layer QG numerical channel flow which is in a statistical steady state. (The potential vorticity (PV) field of the upper layer is shown. Red and blue mark cyclonic and anticyclonic vortices respectively.

and the vortex strength κ. Only two types of vortex streets (symmetric streets with non-shifted rows (figure 1a) and antisymmetric streets with rows shifted by $s = a/2$ (figure 1b) are able to move themselves as a stationary structure with constant speed c in the zonal direction (x-direction). Basically antisymmetric streets are observed. The model of symmetric streets is important to describe the flow consisting of a row of cyclones or anticyclones along a wall, i.e. a single vortex street along a coastline in the ocean.

Von Kármán vortex streets can arise in two different ways: as trapped streets downstream of obstacles placed in a uniform oncoming steady flow; and as freely propagating streets in zonal jet-like flows. Vortex streets trapped behind obstacles have been intensively studied during the last hundred years in a huge number of laboratory experiments starting from Bénard (1908), see e.g. Durgin & Karlson (1971) and references therein. With satellite imagery it was realized that trapped vortex streets also existed on much larger scales in the atmosphere behind mountains (see e.g. Etling 1989 and references therein). Measurements from ship revealed further that the same phenomenon could be found behind islands in the ocean (see e.g. Barkley 1972). Freely propagating vortex streets were observed in geophysical flows on even larger scales, as for example in the ocean (Barkley 1968) on Jupiter (Ingersoll 1990; Marcus & Lee 1998) and on Saturn (Godfrey, Hunt & Suomi 1983). Finally, von Kármán streets were also used to interpret patterns observed in planetary and interplanetary plasmas, as for example those observed in black aurora (see Shukla, Birk & Bingham 1985 and Kimball & Hallinan 1998) or in the heliosphere (see Burlaga 1990).

More recently von Kármán vortex streets have been intensively studied numerically. Freely propagating von Kármán vortex streets were reproduced in two-dimensional flows by Aref & Siggia (1981) and in large-scale geophysical flows affected by rotation by Flierl, Malanotte-Rizzoli & Zabusky (1987), Gurulev & Kozlov (1988), Borth (1999) and Poulin & Flierl (2003). Figure 2 is an example of a freely propagating von Kármán street which self-organized in a turbulent large-scale geophysical flow affected by rotation and stratification (Borth 1999 and Borth *et al.* 2004). Shown is a representative snapshot of the potential vorticity (PV) field of the intermittent turbulent jets typically arising in the statistically steady regime of a wind-driven two-layer numerical channel flow with vanishing or weak ambient vorticity gradient.

The periodically arranged cyclones and anticyclones with the horizontal flow topology of an antisymmetric vortex street (figure 1*b*) organize themselves from a wind-driven disordered flow and persist for all time.

The persistence of von Kármán streets can be explained by the mechanism of locking together many vortices through a self-sustaining superposition of the flow fields of the individual vortices resulting in a large-scale periodic structure of special symmetry moving as a whole with constant zonal speed (Kármán 1911; Lamb 1932). The classical von Kármán theory of vortex streets based on the point vortex approach and the more recent theories considering vortices of finite size (Saffman & Schatzman 1981, 1982) do not take into account stratification and differential rotation effects. The effect of stratification on the structure and dynamics of von Kármán vortex streets in a QG (quasi-geostrophic) equivalent barotropic (1 1/2)-layer model of point vortices on the f-plane was considered by Stewart (1945) and by Masuda & Miki (1995). They both give an exact solution for symmetric and antisymmetric von Kármán vortex streets. The effect of differential rotation on the structure and dynamics of von Kármán vortex streets was investigated by Gryanik (1986) in the framework of the point vortex approximation, but only the case of barotropic flows was considered. These theories assume a homogeneous vertical structure of the localized vortices, which is not the case in baroclinic flows where vortices can be of different vertical extent. Two basic cases of baroclinic vortex streets can be distinguished: mechanically driven upper-layer streets which can be generated by wind stress in the ocean (see figure 2) and thermally driven hetonic streets, which can be naturally generated, e.g. in deep convection.

In our idealized model description these two cases is represented by upper-layer streets (figure 3*b*, below) and hetonic streets (figure 3*c*, below) respectively.

The basic idea of the present study is to generalize the theory of two-dimensional von Kármán streets to a minimal model (a QG two-layer beta-plane) which explicitly resolves the vertical structure of baroclinic vortices and allows the analysis of the combined effects of stratification and differential rotation.

The following problems will be the centre of interest: under which conditions is the self-organization of localized vortices into stationary von-Kármán-like vortex streets in stratified and differentially rotating geophysical flows possible; and how is the dynamics of von Kármán vortex streets affected by external and internal parameters like stratification, differential rotation, intermittency, strength of vortices and vertical structure of vortices.

1.2. *Approach and method*

In real geophysical conditions von-Kármán-type coherent vortex structures develop in very high-Reynolds-number turbulent flows where forcing, dissipation and background fluctuations are always present. We use the adiabatic vortex dynamics approach neglecting effects of forcing and dissipation to tackle the difficult problem of structured turbulence. This approach, suited to describing the nonlinear coherent vortex dynamics effects in turbulence explicitly, has been used before in both homogeneous and isotropic three-dimensional (Biot-Savart vortex filament approximation, e.g. Fernandez, Zabusky & Gryanik 1995; Pullin & Saffman 1998 and references therein) and QG quasi-two-dimensional stratified and rotating (contour dynamics approximation, e.g. Sokolovskiy and Verron 2000 and references therein; point vortex approximation, e.g. Flierl 1987; Gryanik *et al.* 2000 and references therein) turbulent flows. The recent status of the adiabatic vortex dynamics approach to turbulence is discussed in the review of Pullin & Saffman (1998).

For large-scale motions of fast rotating fluids (atmosphere or ocean) the so-called QG two-layer beta-plane model (Phillips model, see Pedlosky 1987) is accepted to be a minimal model. It is designed to describe large-scale fast rotating stably stratified flows, incorporating in elementary form the effects of background stratification by two immiscible fluid layers and planetary rotation by a constant gradient of the rotation rate (Coriolis parameter) in the meridional direction. To investigate von Kármán vortex streets in the QG two-layer beta-plane model we use the approach of baroclinic QG point (singular) vortices. The theory of baroclinic point vortices for two-layer QG flows on the f-plane (constant rotation) was developed by Gryanik (1983) and Hogg & Stommel (1985), see also Legg & Marshall (1993) and Danilov, Gryanik & Olbers (2001). It was generalized further to a beta-plane by Reznik, Grimshaw & Sriskandarajan (1997). The theory of QG two-layer beta-plane vortex streets we develop is based on the model of Reznik *et al.* (1997) and is a straightforward generalization of the theory of barotropic von Kármán vortex streets on an infinite beta-plane (Gryanik 1986), on one hand and of the theory of von Kármán vortex streets on a 1 1/2-layer f-plane (Stewart 1945) on the other.

In § 2 the general model framework and the concept of periodic quasi-stationary point vortex structures on beta-plane is presented. In § 3 the special classes of symmetric and antisymmetric vortex streets with three different vertical structures are introduced. After a description of the scales and characteristic non-dimensional parameters in § 4 the dynamical properties of these streets are analysed in §§ 5 to 7, emphasizing the joint effects of differential rotation and stratification. The basic tool of analysis in these sections is the nonlinear dispersion relation of QG vortex streets. In § 8 the basic physical concepts of the QG vortex street approach are discussed and a classification of QG vortex streets on a diagram of states summarizes the analytical investigations. Section 9 presents scaling laws for von Kármán street phenomena in oceanic, atmospheric and laboratory conditions. Universality and limitations of the results are discussed in § 10, conclusions and an outlook for the application of the theory of QG vortex streets is given in § 11.

2. The quasi-geostrophic two-layer beta-plane model

2.1. *Basic equations*

The QG two-layer beta-plane model (see e.g. Pedlosky 1987) has two immiscible and homogeneous fluid layers with constant densities ρ_1 and ρ_2 and mean thicknesses H_1 and H_2 bounded by a rigid lid and a flat bottom. The dynamics is governed by the potential vorticity (PV) equations

$$\frac{\partial q_j}{\partial t} + J(\psi_j, q_j) + \beta \frac{\partial \psi_j}{\partial x} = \mathscr{F}_j - \mathscr{S}_j, \tag{2.1}$$

$$q_j = \nabla^2 \psi_j + (-1)^j F_j(\psi_1 - \psi_2) \qquad \text{with} \qquad F_j = \frac{f_0^2}{g' H_j}. \tag{2.2}$$

Here ψ_j ($j = 1, 2$) and q_j are the upper- and lower-layer streamfunctions and PV fields, $J(\psi, \omega) = \partial_x \psi\, \partial_y \omega - \partial_y \psi\, \partial_x \omega$ is the Jacobian, $\nabla^2 \psi = \partial_{xx} \psi + \partial_{yy} \psi$ the two-dimensional Laplacian, $f = f_0 + \beta y$ the Coriolis parameter and $g' = g(\rho_2 - \rho_1)/\rho_0$ the reduced gravity with g the gravitational acceleration, ρ_j the densities of the fluid layers and ρ_0 the mean density of the fluid. Further $\mathscr{F}_j$ and $\mathscr{S}_j$ are vorticity sources and sinks. In view of derivations following later the planetary part of the vorticity $f_0 + \beta y$ was taken out of the PV definition (2.2). The zonal velocity u_j, the meridional velocity v_j

and the displacement of the layer interface η, are given by

$$u_j = -\frac{\partial \psi_j}{\partial y}, \quad v_j = \frac{\partial \psi_j}{\partial x}, \quad \eta = \frac{f_0}{g'}(\psi_1 - \psi_2). \tag{2.3}$$

2.2. *Quasi-stationary point vortex structures*

Restricting the class of solutions to quasi-stationary flows moving with constant speed c in the x-direction (zonal direction)

$$\psi_j(x, y, t) = \psi_j(x - ct, y) \tag{2.4}$$

the PV equations (2.1) and (2.2) can be simplified. Inserting (2.4) in equations (2.1) and (2.2), where vorticity source and sink terms are considered to be in exact balance ($\mathscr{F}_j - \mathscr{S}_j = 0$) and introducing a new time-independent x-coordinate $x - ct$ one obtains

$$-c\frac{\partial Q_j}{\partial x} + J(\psi_j, Q_j) = 0, \tag{2.5}$$

$$Q_j = \nabla^2 \psi_j + (-1)^j F_j(\psi_1 - \psi_2) - \frac{\beta}{c}\psi_j, \tag{2.6}$$

where the first two terms correspond to q_j in equation (2.2).

In the special case of a family $\mathscr{A}$ of point anomalies α of the modified PV field Q_j with positions (x_α, y_α) located in layers j_α and having vorticity strengths κ_α the total modified vorticity distribution in layer j can be written as

$$Q_{j,\mathscr{A}}(x, y) = \sum_{\alpha \in \mathscr{A}} \kappa_\alpha \, \delta(x - x_\alpha)\delta(y - y_\alpha)\, \delta_{jj_\alpha}, \tag{2.7}$$

where $\delta(x)$ is the Dirac function and δ_{jj_α} the Kronecker delta. Solving the modified PV equation (2.6) for $Q_{j,\mathscr{A}}$ gives the streamfunction

$$\psi_{j,\mathscr{A}} = \sum_{\alpha \in \mathscr{A}} \kappa_\alpha \left[U_{j1} U^{-1}_{1j_\alpha} G^{\lambda_1}_\alpha + U_{j2} U^{-1}_{2j_\alpha} G^{\lambda_2}_\alpha \right], \tag{2.8}$$

where $G^{\lambda_k}_\alpha$ are the well-known Green's functions solving the Helmholtz equation

$$(\nabla^2 - \lambda_k^2)\, G^{\lambda_k}_\alpha(x, y) = \delta(x - x_\alpha)\delta(y - y_\alpha) \tag{2.9}$$

on an infinite plane given by

$$G^{\lambda_k}_\alpha = \begin{cases} \dfrac{1}{2\pi} \ln\left(\dfrac{r_\alpha}{L_0}\right), & \lambda_k = 0 \\ -\dfrac{1}{2\pi} K_0(\lambda_k r_\alpha), & \lambda_k \neq 0, \end{cases} \tag{2.10}$$

with $K_n(r)$ the modified Bessel function of order n, $r_\alpha(x, y) = \sqrt{(x - x_\alpha)^2 + (y - y_\alpha)^2}$ the distance from the point vortex α and L_0 a physically grounded external length scale (see e.g. Gryanik 1983). The scaling factors λ_k^2 are the eigenvalues of the modified PV operator in (2.6):

$$\lambda_1^2 = \frac{\beta}{c}, \quad \lambda_2^2 = F_1 + F_2 + \frac{\beta}{c}. \tag{2.11}$$

The coefficients $U_{j,k}U^{-1}_{k,l}$ in equation (2.8) are products of the entries of the transformation matrix $\boldsymbol{U}$ and its inverse $\boldsymbol{U}^{-1}$ which diagonalize the modified PV operator (2.6). The first column of $\boldsymbol{U}$ consists of the eigenvector belonging to the

eigenvalue λ_1^2 (barotropic mode) and the second to the eigenvector belonging to λ_2^2 (baroclinic mode). The square roots λ_1 and λ_2 determine the length scales of the barotropic and baroclinic flow fields induced by the vortices. A necessary condition for the localization of the vortex structures are real length scales λ_k or equivalently positive eigenvalues

$$\lambda_k^2 \geqslant 0, \tag{2.12}$$

otherwise the Green's function in (2.10) has wave-like character. On the f-plane $\lambda_1^2 = 0$.

Inserting the vorticity distributions $Q_{j,\mathscr{A}}$ and the corresponding streamfunctions $\psi_{j,\mathscr{A}}$ in the nonlinear part (2.5) of the vorticity equation gives for every point vortex $\alpha \in \mathscr{A}$ the following conditions of quasi-stationarity:

$$c = -\frac{\partial \psi_{j_\alpha,\mathscr{A}'}}{\partial y}\bigg|_{(x_\alpha, y_\alpha)}, \quad 0 = \frac{\partial \psi_{j_\alpha,\mathscr{A}'}}{\partial x}\bigg|_{(x_\alpha, y_\alpha)}, \tag{2.13}$$

where $\mathscr{A}' = \mathscr{A}/\{\alpha\}$ is the family of point vortices with the vortex α itself excluded. For zonally periodic states $\psi(x, y) = \psi(x + X, y)$ with period X the conditions for quasi-stationarity (2.13) have only to be satisfied for vortices within one period in order to hold for the whole vortex structure. In the case $\beta \neq 0$ these conditions are non-trivial since the velocity fields on the right-hand side of (2.13) depend implicitly on the propagation speed c.

Two types of necessary conditions for the existence of localized quasi-stationary point-vortex structures on a beta-plane can be distinguished.

(i) A local condition necessary for the localization of individual vortices

$$0 < c < \infty \tag{2.14}$$

following from (2.11) and (2.12) guarantees the localization of both the barotropic and baroclinic mode and implies that for $\beta \neq 0$ all quasi-stationary structures formed from localized vortices can move only in the positive x-direction (i.e. to the east). For $\lambda_1^2 = 0$ we have from (2.11) $\beta = 0$. In this case (f-plane) to every solution c of (2.13) there corresponds a solution $-c$ by changing cyclones to anticyclones and anticyclones to cyclones. On the beta-plane this is not true (see also the last paragraph of § 8).

(ii) Global conditions, necessary for the existence of a point vortex structure as a quasi-stationary balanced state, follow from solvability conditions of equations (2.13). Two of the global conditions state that the total modified PV $\mathscr{Q}$ of a vortex structure $\mathscr{A}$ and the zonal momentum $\mathscr{P}_y = \sum_{j=1}^{2} H_j \iint \partial \psi_j / \partial x \, \mathrm{d}x \, \mathrm{d}y$ must be exactly zero:

$$\mathscr{Q} = \sum_{\alpha \in \mathscr{A}} H_{j_\alpha} \kappa_\alpha = 0, \quad \mathscr{P}_y = \sum_{\alpha \in \mathscr{A}} H_{j_\alpha} \kappa_\alpha x_\alpha = 0. \tag{2.15}$$

Both conditions in (2.15) follow from equations (2.13) and integration of equation (2.7) over the layers, using the methods of Gryanik (1986), Reznik (1986) and Flierl (1987). Other known examples of localized quasi-stationary vortex structures on the beta-plane satisfying all the necessary conditions are vortex dipoles (so-called modons) and point vortex pairs, see e.g. reviews of Flierl (1987) and Nycander (1994). For linear Rossby waves $c < 0$ (e.g. Pedlosky 1987), and the localization condition (2.14) is obviously not satisfied.

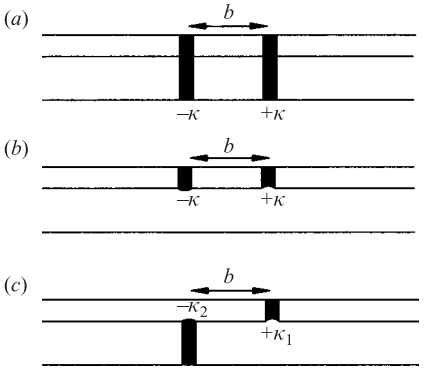

FIGURE 3. Vertical structure of barotropic vortex streets (*a*), vortex streets with vortices in the upper layer (*b*) and hetonic vortex streets (*c*).

3. Three basic types of QG von Kármán streets

By symmetry von Kármán vortex streets (see figures 1 and 2) automatically satisfy the necessary quasi-stationarity conditions (2.15) and the meridional part of the speed relation (2.13). A given von Kármán street can exist as a quasi-stationary state only if the zonal part of the nonlinear speed relation (2.13) has some solution c. We will construct three different types of vortex streets with essentially different transport properties depending on the vertical structure of the individual vortices.

Type I: Barotropic vortex streets (S symmetric, A antisymmetric) consisting of vortices of the same strength κ in both layers (figure 3*a*) have flow fields that stay barotropic forever so that the stratification has no influence. Evaluating equation (2.8) for the modified vorticity distribution of barotropic streets leads to the streamfunction

$$\psi_1(x, y) = \psi_2(x, y) = \kappa \left[G^{\lambda}_{row}(x, y; 0, b/2) - G^{\lambda}_{row}(x, y; s, -b/2)\right] \tag{3.1}$$

where G^{λ}_{row} is the Green's function of a periodic row of vortices. In Appendix A two representations are derived for G^{λ}_{row}: one emphasizing the contributions of the individual vortices

$$G^{\lambda}_{row}(x, y; x_0, y_0) = -\frac{1}{2\pi} \sum_{m=-\infty}^{\infty} K_0(\lambda \sqrt{(x - ma - x_0)^2 + (y - y_0)^2}); \tag{3.2}$$

and a second emphasizing the zonal periodicity structure of the street

$$G^{\lambda}_{row}(x, y; x_0, y_0) = -\frac{1}{a} \sum_{n=-\infty}^{\infty} \frac{\exp(-\sqrt{(2\pi n/a)^2 + \lambda^2}\ |y - y_0|}{\sqrt{(2\pi n/a)^2 + \lambda^2}} \cos \frac{2\pi n}{a}(x - x_0). \tag{3.3}$$

Substituting the first representation of the Green's function into (2.13) we obtain the nonlinear dispersion relation

$$c = \frac{\kappa}{2\pi} \sum_{m=-\infty}^{\infty} \frac{b\lambda}{r_m} K_1(\lambda r_m), \tag{3.4}$$

with $\lambda = (\beta/c)^{1/2}$ the length scale, a the zonal distance between vortices, b the distance between rows and $r_m = ((ma + s)^2 + b^2)^{1/2}$ the distance function ($s = 0$ for symmetric streets and $s = a/2$ for antisymmetric streets). Barotropic vortex streets in two layers are dynamically equivalent to vortex streets in barotropic models (Gryanik 1986).

Type II: Upper-layer vortex streets (S_e symmetric, A_e antisymmetric) with vortices located in the upper layer (figure 3*b*) 'feel' the baroclinic field and equation (2.8) leads to the streamfunction

$$\psi(x,y) = \kappa\left[G^{\lambda_1}_{row}(x,y;0,b/2) - G^{\lambda_1}_{row}(x,y;s,-b/2)\right]\boldsymbol{B} + \kappa\left[G^{\lambda_2}_{row}(x,y;0,b/2) - G^{\lambda_2}_{row}(x,y;s,-b/2)\right]\boldsymbol{C}, \quad (3.5)$$

where $\boldsymbol{B}=(A_1,A_1)$ and $\boldsymbol{C}=(A_2,-A_1)$, with $A_1=1-A_2=H_1/(H_1+H_2)$ and the length scales λ_1 and λ_2 from (2.11). Substituting (3.2) into (2.13) gives the nonlinear dispersion relation

$$c = \frac{\kappa}{2\pi}\sum_{m=-\infty}^{\infty}\frac{b}{r_m}[A_1\lambda_1 K_1(\lambda_1 r_m) + A_2\lambda_2 K_1(\lambda_2 r_m)], \quad (3.6)$$

with G^{λ}_{row}, a, and r_m as in the barotropic case. The specific property of streets with vortices in only one layer is that the globally integrated layer thickness anomaly η vanishes, so that they are generated without heat sources (mechanical production). Upper-layer streets in the limit $\beta=0$ and $F_2/F_1\to 0$ coincide with the 1 1/2-layer vortex streets treated by Stewart (1945) and Masuda & Miki (1995).

Type III: Hetonic vortex streets (S_d symmetric, A_d antisymmetric) with the row of positive vortices located in the upper layer and the row of negative vortices in the lower layer (figure 3*c*) have, due to (2.15), to satisfy the relation $\kappa_1/\kappa_2=-H_2/H_1$. Using equation (2.8) we obtain the streamfunction

$$\psi(x,y) = \kappa\left[G^{\lambda_1}_{row}(x,y;0,b/2) - G^{\lambda_1}_{row}(x,y;s,-b/2)\right]\boldsymbol{B} + \kappa\left[G^{\lambda_2}_{row}(x,y;0,b/2) + \frac{A_1}{A_2}G^{\lambda_2}_{row}(x,y;s,-b/2)\right]\boldsymbol{C}. \quad (3.7)$$

The condition of quasi-stationarity (2.13) reduces using (3.2) to the nonlinear dispersion relation

$$c = \frac{\kappa}{2\pi}\sum_{m=-\infty}^{\infty}\frac{b}{r_m}A_1[\lambda_1 K_1(\lambda_1 r_m) - \lambda_2 K_1(\lambda_2 r_m)]. \quad (3.8)$$

G^{λ}_{row}, s, $\boldsymbol{B}$, $\boldsymbol{C}$, A_1, A_2 and r_m are defined as in the previous cases, (3.4) and (3.6). Hetonic streets carry a net layer thickness anomaly η, which means that heat sources are necessary for their formation (thermal production). For another form of the nonlinear dispersion relations using the second representation see Appendix A.

Purely baroclinic von Kármán streets, i.e. streets formed from two rows of aligned hetons, do not exist as quasi-stationary solutions, since the velocities induced at the positions of anticyclones and the position of cyclones forming the individual hetons are of opposite sign and so will break up the hetons.

4. Scaling and characteristic non-dimensional parameters

Natural length and time scales of von Kármán flow systems are given by $L=a$ and $T=2a^2/\kappa=L/V$, where $V=\kappa/2a$ is the characteristic velocity. So a system of four non-dimensional parameters can be introduced to characterize two-layer QG von Kármán streets on a beta-plane:

$$k=\frac{b}{a}, \quad \epsilon=\frac{2a^3\beta}{\kappa}, \quad \sigma=\frac{a}{R_0}, \quad \delta=\frac{H_1}{H_1+H_2}, \quad (4.1)$$

with $R_0 = \sqrt{g'(H_1 + H_2)}/(2f_0)$ the reference Rossby radius which in the case of equal layers coincides with $R = (F_1 + F_2)^{-1/2}$, where $R = 2R_0\sqrt{\delta(1-\delta)}$.

The horizontal aspect ratio k characterizes the density of vortices along the rows of streets. Vortex streets with $k \ll 1$ will be called, 'dilute streets', and in the opposite limiting case $k \gg 1$ 'dense streets'. Symmetric dilute streets behave like vortex pairs and dense vortex streets like two parallel vortex sheets.

The planetary (ambient) vorticity gradient ϵ characterizes the effects of differential background rotation, so that the case $\epsilon = 0$ corresponds to f-plane streets.

The two parameters σ and δ characterize the joint effects of homogenous rotation and stratification. The cases $\sigma = 0$ and $\sigma = \infty$ correspond to barotropic and equivalent barotropic streets respectively, otherwise streets are called baroclinic. The equivalent barotropic limit describes two uncoupled layers (Pedlosky 1987).

Using the system (4.1) of non-dimensional parameters and the velocity scale V the propagation speed can now be written as

$$c = V\, C(k, \epsilon, \sigma, \delta). \tag{4.2}$$

Vortex streets propagating with speeds $C < C_{crit}$ and $C > C_{crit}$ are called 'slow' and 'fast' streets respectively, where $C_{crit} = C_{crit}(\epsilon, \sigma, \delta)$ is a critical speed which will be determined explicitly in §§ 5 to 7.

5. Barotropic vortex streets

Barotropic vortex streets S and A can exist as quasi-stationary states if to a given set of parameters there exist solutions of the speed equation (3.4). Using the non-dimensional parameters introduced in (4.1) one can write

$$C = \frac{1}{\pi}\sqrt{\frac{\epsilon}{C}} \sum_{m=-\infty}^{\infty} \frac{1}{r_m(k)}\, K_1\left(k\sqrt{\frac{\epsilon}{C}}\, r_m(k)\right), \tag{5.1}$$

with the non-dimensional distance function $r_m(k) = \sqrt{1 + ((m+s)/k)^2}$ ($s = 0$ for symmetric streets and $s = 1/2$ for antisymmetric streets). The propagation speed C is given implicitly and a unique analytical relationship $C = C(k, \epsilon)$ cannot be given in general.

Only in the limit of vanishing planetary vorticity gradient $\epsilon = 0$ (f-plane) can equation (5.1) be solved explicitly:

$$C = \cosh \pi k, \quad C = \tanh \pi k, \tag{5.2}$$

giving the well-known propagation speed of classical symmetric and antisymmetric von Kármán streets in two-dimensional flows represented as dashed lines in plots (a) and (c) of figure 4.

For $\epsilon \neq 0$ symmetric streets (figure 4a) can exist as quasi-stationary states only if k is below or equal to some critical maximum aspect ratio k_{max}. In the case $\epsilon = 5$ in figure 4(a) one can estimate k_{max} by using the dispersion relation (5.1) in the limit of dilute vortex streets obtained by considering only the contribution of the nearest vortex given by the term $m = 0$. The asymptotic expressions for the maximum critical aspect ratio k_{max} and the critical speed C_{crit} are

$$k_{max} = \left(\frac{\xi_0^3 K_1(\xi_0)}{\pi}\right)^{1/3} \epsilon^{-1/3} \approx 0.717\, \epsilon^{-1/3}, \quad C_{crit} \approx 0.065\, k_{max}^{-1}, \tag{5.3}$$

where $\xi = k\sqrt{\epsilon/C}$ and the function $\xi^3 K_1(\xi)$ attains its maximum for $\xi_0 \sim 2.387$.

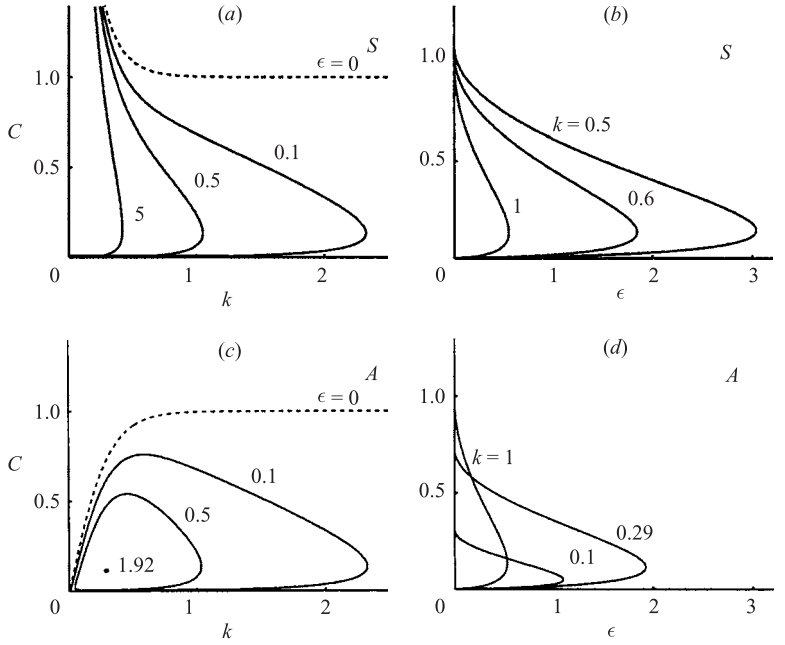

FIGURE 4. Dispersion relation for barotropic vortex streets. Speed C as function of k for different ϵ: (*a*) symmetric streets, (*c*) antisymmetric streets. Speed C as function of ϵ for different k: (*b*) symmetric streets, (*d*) antisymmetric streets.

The propagation speed of fast dilute vortex streets can be approximated by

$$C = \frac{1}{\pi k} - \frac{k^2\epsilon}{4} \ln\left(\frac{4}{\pi\epsilon k^3}\right) \quad \text{if} \quad k\sqrt{\epsilon/C} \ll 1, \tag{5.4}$$

where the first term is the propagation speed of a vortex pair on the f-plane (dashed curve in figure 4*a*) and the second term is a non-analytical correction. The correction is always negative since $4/(\pi\epsilon k^3) \gg 1$. The propagation speed of slow dilute vortex streets (lower branch of solution curves) is given by

$$C = \frac{k^2\epsilon}{\ln^2(1/\sqrt{2\pi}k^3\epsilon)}\left(1 - 5\,\frac{\ln\ln(1/\sqrt{2\pi}k^3\epsilon)}{\ln(1/\sqrt{2\pi}k^3\epsilon)}\right) \tag{5.5}$$

and valid for $k\sqrt{\epsilon/C} \gg 1$ and $k \ll \min(1, \epsilon^{-1/3})$. Slow dilute symmetric vortex streets are generic beta-plane solutions and have no analogue on the f-plane.

The critical maximum aspect ratio k_{max} for the $\epsilon = 0.1$ curve in figure 4(*a*) can be estimated by using the dispersion relation (5.1) in the dense street approximation obtained by keeping only the first term of the second representation of the dispersion relation (B 3) or (B 5) in Appendix B. For k_{max} and the corresponding critical propagation speed one obtains the following asymptotic expressions:

$$k_{max} = \frac{2}{\mathrm{e}}\epsilon^{-1/2}, \quad C = \mathrm{e}^{-2}. \tag{5.6}$$

The propagation speed of fast dense vortex streets is

$$C = 1 - k\sqrt{\epsilon} \quad \text{if} \quad k\sqrt{\epsilon/C} \ll 1. \tag{5.7}$$

The linear behaviour in k can be clearly seen in figure 4(*a*). The propagation speed of slow dense vortex streets is estimated for $k\sqrt{\epsilon/C} \gg 1$ by the asymptotic formula (5.5) where the arguments in the logarithms are replaced by $1/(k^2\epsilon)$ and the factor in front of the second term in the bracket is 4. As shown in figure 4, increasing ϵ decreases the critical aspect ratio k_{max} so that for a stronger ϵ only more pair-like symmetric streets survive. Since by our choice of non-dimensional parameters the vorticity density per unit length along vortex rows is fixed, this means that for increasing ϵ the vorticity has to be concentrated in a smaller number of stronger vortices. Another possibility of course would be to consider vortex streets with a larger vorticity density per unit length. For aspect ratios smaller than the critical maximum aspect ratio $k < k_{max}$ there are always two solutions: a fast vortex street (upper branch of the curves) and a slow one (lower branch). If we fix the aspect ratio (see figure 4*b*) a symmetric street can only exist for values of ϵ smaller than a critical maximum $\epsilon_{max}(k)$ which for decreasing aspect ratio becomes larger. Fast symmetric streets propagate in the limit $\epsilon \to 0$ with the same speed as the corresponding f-plane streets (points where the upper branches in figure 4*b* meet the C-axis) and slow symmetric streets approach zero propagation speed for all aspect ratios.

For antisymmetric vortex streets, in addition to the critical maximum aspect ratio k_{max} a critical minimum aspect ratio k_{min} also exists below which no quasi-stationarity is possible (figure 4*c*). The minimum critical aspect ratios k_{min} for the solution curves can be derived for dilute antisymmetric streets ($k \ll 1$ and $\sqrt{\epsilon/C} \gg 1$). Keeping the contributions of the two nearest neighbours in equation (5.1) one obtains

$$k_{min} = \frac{\pi}{32\xi_0^3 K_1(\xi_0)}\epsilon \approx 0.085\epsilon, \quad C_{crit} \approx 0.517\, k_{min}, \tag{5.8}$$

where the function $\xi^3 K_1(\xi)$ has its maximum at $\xi_0 = \sqrt{\epsilon/4C}$. For increasing ϵ numerical summing of the full formula is needed to describe the details. The qualitative behaviour follows immediately: increasing ϵ induces decreasing maximum critical aspect ratios and increasing minimum critical aspect ratios till the solution curve reduces to one point. The minimum and maximum critical aspect ratios meet at $k_{crit} \sim 0.29$ for $\epsilon_{crit} \sim 1.92$. An important new feature is that now $\epsilon_{crit} \sim 1.92$ is a global critical value so that no antisymmetric street can exist when we increase ϵ beyond this value. The propagation speed of antisymmetric streets increases for $\epsilon = 0$ monotonically with increasing aspect ratio k. For $\epsilon > 0$ the propagation speed $C(k)$ of the fast branch is no longer monotonic and has a finite maximum depending on ϵ. Figure 4(*d*) illustrates that antisymmetric streets with aspect ratios near the critical value $k \sim 0.29$ can survive for the strongest planetary (ambient) vorticity gradient.

Figure 5 gives an overview of the parameters on the (k, ϵ)-plane where barotropic vortex streets can exist as quasi-stationary states on the beta-plane. The dashed line represents the critical maximum aspect ratio as a function of ϵ for symmetric vortex streets and the solid line the corresponding critical maximum (upper branch) and critical minimum (lower branch) aspect ratios for antisymmetric streets. Above the dashed line there are no vortex street solutions, on the dashed line there exists one symmetric street and below it there are two symmetric streets (S). For increasing ϵ, as already mentioned, only more and more pair-like symmetric vortex streets survive. The domain where antisymmetric streets can exist (delimited by the solid line) is always below the dashed critical curve of symmetric streets and does not penetrate into regions with planetary (ambient) vorticity gradients larger than $\epsilon = 1.92$. This

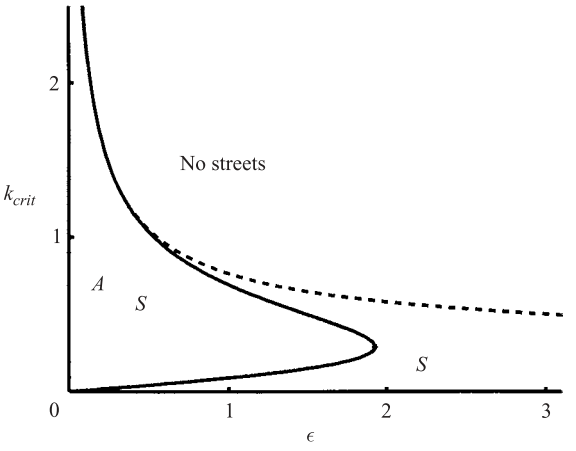

FIGURE 5. Critical aspect ratio k_{crit} as function of ϵ for barotropic streets. The dashed line represents the critical curve for symmetric streets and the solid line for antisymmetric streets.

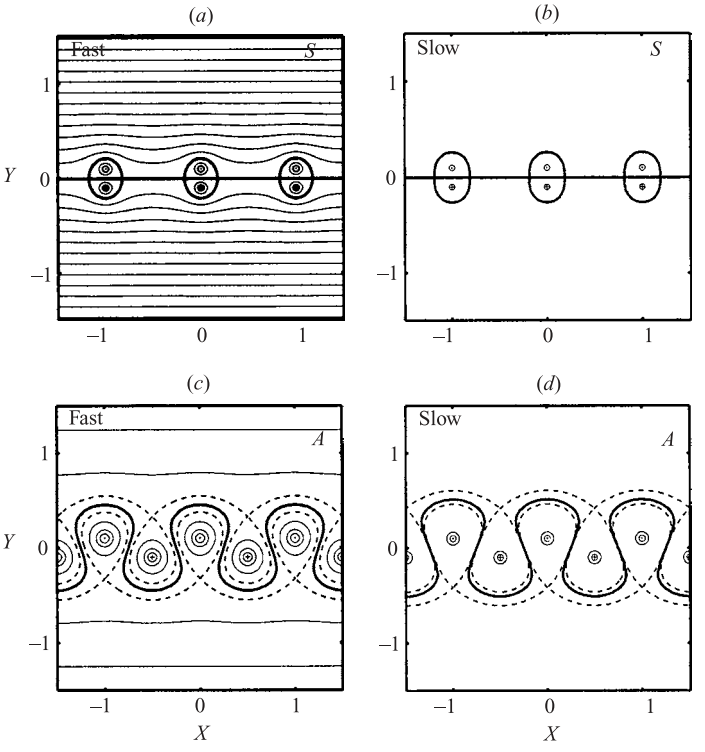

FIGURE 6. Streamline topologies of fast and slow barotropic vortex streets belonging to the same set of parameters ($k = 0.2$ and $\epsilon = 0.5$). (a, b) Fast and slow symmetric street. (c, d) Fast and slow antisymmetric street.

diagram reveals that increasing ϵ focuses the aspect ratios of possible vortex streets into a narrow range.

To illustrate the properties of the beta-plane vortex street solutions the streamline topologies of a modon-type symmetric and a strongly meandering antisymmetric vortex street are presented in figure 6. Non-dimensional comoving streamfunctions

$\Phi = \Psi(X, Y) + CY$ are used, where Ψ/κ, $X = x/a$ and $Y = y/a$. Shown are a fast and a slow solution belonging to the same set of parameters. For larger aspect ratios k a topological transition leads to a zonally connected flow with different fluid cells in the symmetric and antisymmetric case (not shown).

6. Vortex streets with vortices in the upper layer

Using the non-dimensional parameters defined in (4.1) the nonlinear dispersion relation (3.6) for symmetric S_e and antisymmetric A_e streets with vortices in the upper layer can be written in the form

$$C = \frac{1}{\pi} \sum_{m=-\infty}^{\infty} \frac{1}{r_m(k)} \left[\delta \sqrt{\frac{\epsilon}{C}} K_1 \left(k \sqrt{\frac{\epsilon}{C}} r_m(k) \right) + (1-\delta) \sqrt{\frac{\epsilon}{C} + \frac{\sigma^2}{4\delta(1-\delta)}} K_1 \left(k \sqrt{\frac{\epsilon}{C} + \frac{\sigma^2}{4\delta(1-\delta)}} r_m(k) \right) \right]. \quad (6.1)$$

The distance function $r_m(k)$ is the same as for the barotropic streets in equation (5.1).

In the limit $\epsilon = 0$ the nonlinear dispersion relation (6.1) can be explicitly solved for C. For symmetric streets we obtain

$$C = \delta \coth \pi k + \frac{\sigma}{2\pi} \sqrt{\frac{1-\delta}{\delta}} \left[K_1 \left(\frac{\sigma k}{2\sqrt{\delta(1-\delta)}} \right) + 2 \sum_{m=1}^{\infty} \frac{1}{r_m(k)} K_1 \left(\frac{\sigma k r_m(k)}{2\sqrt{\delta(1-\delta)}} \right) \right], \quad (6.2)$$

with the distance function $r_m(k)$ of (6.1) taken for $s = 0$. In the case of antisymmetric streets we obtain

$$C = \delta \tanh \pi k + \frac{\sigma}{\pi} \sqrt{\frac{1-\delta}{\delta}} \sum_{m=0}^{\infty} \frac{1}{r_m(k)} K_1 \left(\frac{\sigma k r_m(k)}{2\sqrt{\delta(1-\delta)}} \right), \quad (6.3)$$

with the distance function $r_m(k)$ of (6.1) taken for $s = 1/2$. In figures 7(a) and 7(c) the propagation speeds (6.2) and (6.3) of symmetric and antisymmetric streets are represented as functions of the aspect ratio k. The upper dashed lines ($\sigma = 0$), represent barotropic streets and the lower dashed lines equivalent barotropic streets ($\sigma = \infty$). The specific behaviour of the baroclinic flow field occurs only for intermediate values of σ at which the vortex system evolves at scales comparable to the Rossby radius R_0. The general behaviour can be seen from figures 7(b) and 7(d) where the propagation speed C is plotted for different aspect ratios k as a function of σ.

At intermediate values of stratification–rotation parameters σ the speed of propagation of symmetric dilute streets is approximated by

$$C = \frac{\delta}{\pi k} + \frac{\sigma}{2\pi} \sqrt{\frac{1-\delta}{\delta}} K_1 \left(\frac{\sigma k}{2\sqrt{\delta(1-\delta)}} \right). \quad (6.4)$$

Dense vortex streets propagate with the speed

$$C = \delta + (1-\delta) \exp \left(-\frac{\sigma k}{2\sqrt{\delta(1-\delta)}} \right). \quad (6.5)$$

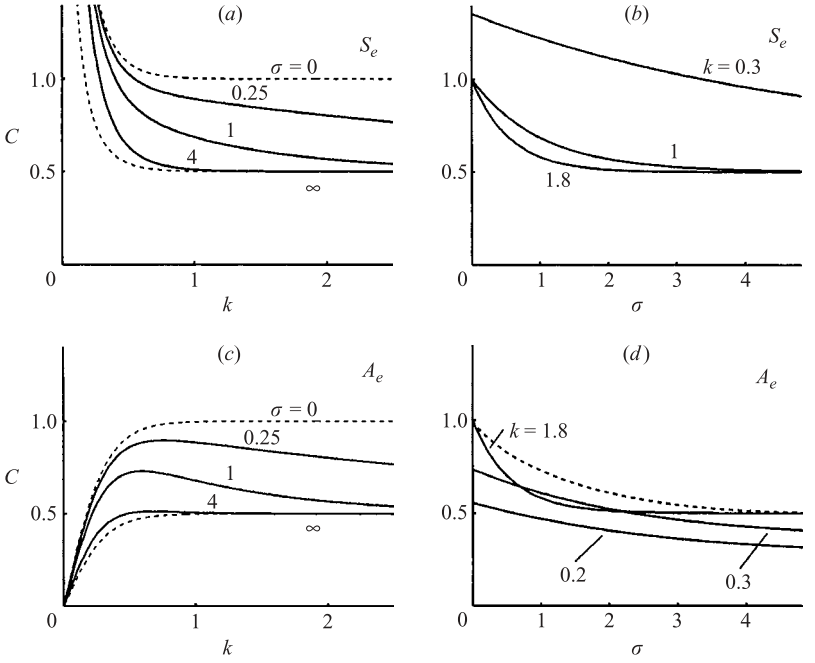

FIGURE 7. Dispersion relation for upper-layer vortex streets for $\epsilon = 0$ and $\delta = 0.5$. Speed C as a function of k for symmetric (a) and antisymmetric streets (c). Speed C as a function of σ for symmetric (b) and antisymmetric streets (d). The dashed line in (d) represents the maximum speed C_{max} with which the fastest antisymmetric street can propagate for a given σ.

For increasing k or σ the speed approaches the barotropic limit $C = \delta$. For decreasing σ and fixed k the equivalent barotropic limit with $C = 1$ is always attained.

The speed $C(k)$ of antisymmetric streets shows, unlike barotropic streets, a non-monotonic behaviour so that there exists a finite aspect ratio k_0 at which a maximum speed C_{max} is reached. For small aspect ratios ($k \ll 1$) antisymmetric streets accelerate with increasing aspect ratios following the curve of the small-scale limit ($\sigma = 0$). The asymptotic formula is given by

$$C = \delta\pi k + \frac{2k\sigma}{\pi}\sqrt{\frac{1-\delta}{\delta}}\,K_1\left(\frac{\sigma}{4\sqrt{\delta(1-\delta)}}\right). \tag{6.6}$$

After having reached the maximum speed C_{max}, which is reached later with decreasing σ, they slow down again if the aspect ratio k is increased further till they approach the equivalent barotropic sheet limit $C = \delta$ ($\sigma = \infty$). The asymptotics is the same as for dense symmetric streets given in (6.5). The smaller the relative thickness of the upper layer the stronger the non-monotonic behaviour. This non-monotonic behaviour of C of antisymmetric streets is due to the combination of two effects. First the transition from a regime where only adjacent vortices influence each other (dilute limit) to a regime where vortices are influenced by the mean field of a large number of vortices (dense limit). Second the clustering of vortices into groups if they are located in an area with a diameter comparable to the Rossby radius. If vortices in the dilute regime are at distances apart much larger than the Rossby radius (lowest solid curves in figure 7c) the propagation speed follows closely the curve of the barotropic large-scale limit and the non-monotonicity is not pronounced. If on the other hand

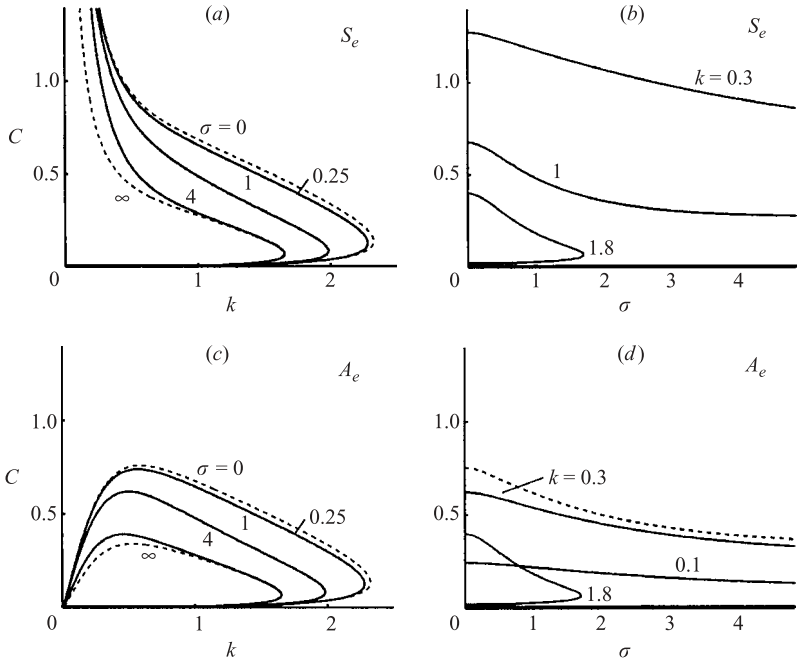

FIGURE 8. Same as figure 7 but for $\epsilon = 0.1$.

the transition between the dilute and dense regimes occurs at distances which are much larger than the Rossby radius (upper solid curve in figure 7*c*) the propagation speed follows more closely the dashed curve of the barotropic limit. It drops slowly and approaches the equivalent barotropic limit for aspect ratios k where the vortex rows are at larger distances apart than the Rossby radius. The non-monotonicity is most pronounced if the transition between dilute and dense regimes occurs at vortex separations comparable to the Rossby radius (solid curve in the middle of figure 7*c*). The non-monotonicity is clearly seen in figure 7(*d*). The upper dashed curve represents the speed C_{max} which for given σ is reached by the fastest antisymmetric street.

The general properties of the solutions $C(k, \epsilon, \sigma, \delta)$ of equation (6.1) for $\epsilon \neq 0$ are summarized in figures 8 and 9. Comparing figures 8(*a*) and 8(*c*) to the corresponding figures 4(*a*) and 4(*c*) for barotropic streets we notice that the domain of existence shrinks with increasing stratification σ. For aspect ratios which are within the non-critical interval $(0, k_{max})$ for symmetric streets and (k_{min}, k_{max}) for antisymmetric streets a fast and a slow solution can again be found. In figures 8(*a*) and 8(*c*) we have chosen $\epsilon = 0.1$ so that the equivalent barotropic limit ($\sigma = 0$) (upper dashed line) corresponds to the first case represented in figures 4(*a*) and 4(*c*). We see that for intermediate aspect ratios an increasing σ acts qualitatively like an increasing ϵ and that all curves lie between the barotropic ($\sigma = 0$) and equivalent barotropic ($\sigma = \infty$) limit as in the case of vanishing $\epsilon = 0$ in figures 7(*a*) and 7(*c*).

Since in the limit $\sigma \to 0$ the dispersion relation (6.1) reduces exactly to the barotropic relation (5.1) all formulae derived for barotropic streets are in this case also valid for upper-layer streets. In the limit $\sigma \to \infty$ the dispersion relation (6.1) reduces to the barotropic relation (5.1) weighted by the relative thickness δ of the first layer. Using (5.3) for the critical maximum aspect ratio of dilute symmetric upper-layer streets we

find

$$\left(\frac{\xi_0^3 K_1(\xi_0)}{\pi}\right)^{1/3} \delta^{1/3}\,\epsilon^{-1/3} \leqslant k_{max} \leqslant \left(\frac{\xi_0^3 K_1(\xi_0)}{\pi}\right)^{1/3} \epsilon^{-1/3}, \tag{6.7}$$

where for large σ the lower limit is approached and for small σ the upper. Similarly the critical minimum aspect ratio k_{min} for dilute antisymmetric streets can be estimated using (5.8). For all σ one has the interval

$$\frac{\pi}{32\xi_0^3 K_1(\xi_0)}\,\epsilon \leqslant k_{min} \leqslant \frac{\pi}{32\xi_0^3 K_1(\xi_0)}\,\delta^{-1}\,\epsilon, \tag{6.8}$$

with the lower bound approached for small σ and the upper for large σ. The limit of dense barotropic vortex streets (5.6) allows the critical maximum aspect ratio k_{max} to be estimated for symmetric and antisymmetric upper-layer streets:

$$\frac{2}{\mathrm{e}}\,\delta^{1/2}\,\epsilon^{-1/2} \leqslant k_{max} \leqslant \frac{2}{\mathrm{e}}\,\epsilon^{-1/2}. \tag{6.9}$$

For fast dilute symmetric streets we obtain the approximate formula

$$C = C_f - \delta\frac{\epsilon k}{4\pi C_f}\,\ln\frac{4C_f}{\epsilon k^2} \quad \text{for} \quad k\sqrt{\epsilon/C} \ll 1 \quad \text{and} \quad \epsilon/C \ll \sigma^2/(4\delta(1-\delta)), \tag{6.10}$$

where C_f is given by (6.4). The correction is always negative since the argument in the logarithm is very large. If one replaces C_f by the propagation speed of pair-like barotropic vortex streets, formula (6.10) reduces to the corresponding barotropic equation (5.4) except for the weighting factor δ in the correction term. Changing the second condition of (6.10) to $\epsilon/C \gg \sigma^2/(4\delta(1-\delta))$ and keeping the first, i.e. if we look for small corrections of the barotropic beta-plane solutions due to stratification, we obtain

$$C = C_\beta - \frac{k\sigma^2}{16\pi\delta}\,\ln\frac{4}{\pi k^3 \epsilon}, \tag{6.11}$$

where C_β is the propagation speed of dilute barotropic streets given in equation (5.4).

The influence of stratification on the propagation speed of slow streets is given by

$$C = C_\beta\left(1 + C_\beta\frac{\sigma^2}{4\delta\epsilon}\right) \quad \text{for} \quad k\sqrt{\epsilon/C} \gg 1 \quad \text{and} \quad \sigma^2/(4\delta(1-\delta)) \ll \epsilon/C, \tag{6.12}$$

where C_β is the propagation speed of barotropic streets given in (5.5). The correction terms in (6.11) and (6.12) show a parabolic behaviour ($\sim\sigma^2$), which can also clearly be seen for small stratifications in figures 8(b) and 8(d).

The propagation speed of dense fast vortex streets

$$C = C_f - \delta k\sqrt{\frac{\epsilon}{C_f}} \quad \text{for} \quad k\sqrt{\epsilon/C} \ll 1 \quad \text{and} \quad \epsilon/C \ll \sigma/(4\delta(1-\delta)) \tag{6.13}$$

is a good approximation for the slope of the curves around $k = 1$ in figures 8(a) and 8(c) as long as $\sigma > 1$. The stratification correction for the propagation speed of slow dense upper-layer vortex streets has, assuming $\sigma/(2\sqrt{\delta(1-\delta)}) \ll \epsilon/C$, the same relation as for dilute streets (6.12), but the barotropic speed C_β of dense vortex streets has to be taken.

The effect of stratification on the propagation speed C of fast barotropic antisymmetric streets is most pronounced for the curve for $\sigma = 1$ in figure 8(c). The slope for fast streets for aspect ratios $k > k_0$ is steeper than for the case without stratification and only flattens out when the critical aspect ratio k_{max} is approached.

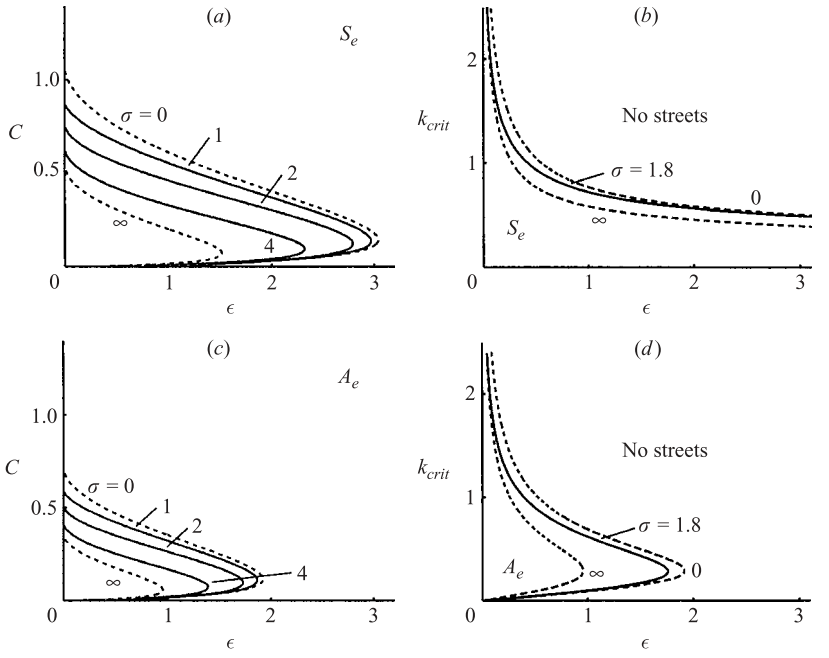

FIGURE 9. Dispersion relation for upper-layer vortex streets. Speed C as function of ϵ for different σ : (a) symmetric streets, (c) antisymmetric streets Critical aspect ratio k_{crit} as function of ϵ : (b) symmetric streets, (d) antisymmetric streets.

Figures 9(b) and 9(d) show the propagation speed C as a function of ϵ for different σ and fixed k, corresponding to figures 4(b) and 4(d). For all stratification–rotation parameters σ the solutions C are between the two limiting cases $\sigma = 0$ (upper dashed line) and $\sigma = \infty$ (lower dashed line). As in the barotropic case there is a critical maximum ϵ_{crit} depending on the aspect ratio k. For increasing σ and decreasing relative thickness of the upper layer it decreases and for a given δ reaches its minimum value for $\sigma = \infty$. When ϵ_{crit} is approached the propagation speeds reach the equivalent barotropic limit $\sigma = 0$. For $\epsilon \to 0$ the fast streets tend to the speed $C(k, \sigma)$ of the corresponding vortex streets on the f-plane given by equations (6.2) and (6.3). There can exist a critical stratification σ_{crit} (curves for $k = 1.8$ in figures 8b and 8d) when the aspect ratio of the vortex street lies between the critical aspect ratios of the corresponding barotropic and equivalent barotropic limits $\sigma = 0$ and $\sigma = \infty$ (see figures 8a and 8c). If the aspect ratio k is inside the non-critical interval of the solutions for $\sigma = \infty$ (e.g. $k = 0.3$) then there is no critical stratification and fast and slow solutions always exist (the curves of the slow solutions are too close to the σ-axis to be distinguished). The dashed line in figure 8(d) is the maximum speed which can be reached by antisymmetric streets for given ϵ, σ and δ. As shown in figures 9(b) and 9(d), at large σ the intervals of non-critical aspect ratios are reduced. The same is true for smaller δ. The critical aspect ratios of symmetric streets are closer to the critical aspect ratios of the equivalent barotropic limit $\sigma = \infty$ for small ϵ and closer to those of the barotropic limit $\sigma = 0$ for larger ϵ.

Thus the stratification–rotation parameter σ and the aspect ratio of layer thicknesses δ have a very strong influence on the structure and dynamics of upper-layer streets.

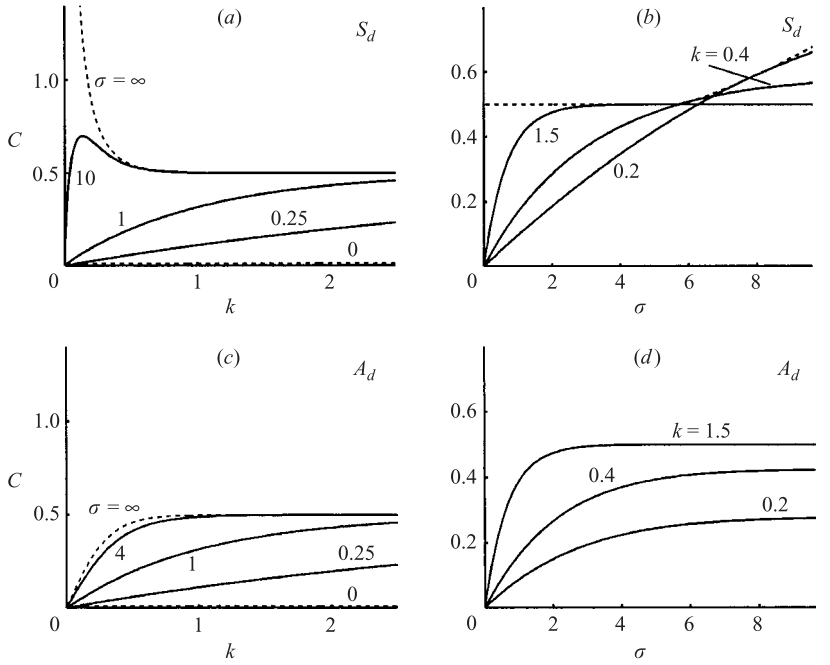

FIGURE 10. Dispersion relation for hetonic vortex streets on the f-plane. Same parameters and notation as in figure 7. The dashed line in (b) represents the speed C_{max} at which the fastest symmetric street can move for a given σ.

7. Hetonic vortex streets

The nonlinear dispersion relation (3.8) for symmetric S_d and antisymmetric A_d hetonic vortex streets is given by

$$C = \frac{1}{\pi}\sum_{m=-\infty}^{\infty}\frac{1}{r_m(k)}\left[\delta\sqrt{\frac{\epsilon}{C}}K_1\left(k\sqrt{\frac{\epsilon}{C}}r_m(k)\right)\right.$$
$$\left. - \delta\sqrt{\frac{\epsilon}{C}+\frac{\sigma^2}{4\delta(1-\delta)}}K_1\left(k\sqrt{\frac{\epsilon}{C}+\frac{\sigma^2}{4\delta(1-\delta)}}\,r_m(k)\right)\right]. \quad (7.1)$$

The barotropic contributions to the propagation speed of hetonic streets (first term) is the same as for vortex streets with vortices in the upper layer (6.1) but the factor $1-\delta$ in front of the baroclinic part is replaced by $-\delta$.

As for upper-layer streets an explicit solution for the propagation speed C can be obtained for $\epsilon = 0$. For symmetric streets C is given by the expression (6.3) for upper-layer streets where the second term in brackets has to be multiplied by the factor $-\delta/(1-\delta)$. The same multiplication of the second term in equation (6.2) gives the propagation speed for hetonic antisymmetric streets. Hetonic vortex streets always move slower than the corresponding upper-layer streets: compare figures 7 and 10.

Only in the equivalent barotropic limit does the speed of hetonic streets approach the speed of upper-layer streets. The propagation speed of dilute symmetric hetonic streets is given by (6.4) where the second term has to be multiplied by the factor $-\delta/(1-\delta)$. In this case the propagation speed has a pronounced non-monotonic behaviour, which is a specific effect of baroclinicity and has a local maximum $C_0 = 0.2\,\sigma\sqrt{\delta/1-\delta}$ for the

aspect ratio $k_0 = 2.2\sqrt{\delta(1-\delta)}/\sigma$. Expressed in dimensional variables this means that a heton moves with a maximum speed of $c_0 = 0.2\,\delta\,\kappa/R$ when the horizontal distance between the vortices is of the order of the baroclinic Rossby radius of the system ($b_0 = 1.1\,R$). The approximation

$$C = -\frac{\sigma^2 k}{8\pi(1-\delta)} \ln\left(\frac{\sigma k}{4\sqrt{\delta(1-\delta)}}\right) \quad \text{for} \quad \sigma k/(4\sqrt{\delta(1-\delta)}) \ll 1 \tag{7.2}$$

shows that the velocity can increase arbitrarily for small aspect ratios k. In the limit $\sigma \ll 1$ the heton does not move at all and in the limit $\sigma \gg 1$ it behaves as an upper-layer vortex pair moving with the speed $C = \delta/(\pi k)$.

Dilute antisymmetric streets do not show a non-monotonic behaviour of the propagation speed. To first order the speed increases linearly with k following the relation (6.6) with the standard replacement for the second term, i.e. the multiplication with the factor $-\delta/(1-\delta)$. Also, in the limit of dense vortex streets the propagation speed no longer exhibits a non-monotonic behaviour in the symmetric as well as in the antisymmetric case. The limiting formula is

$$C = \delta - \delta \exp\left(-\frac{\sigma k}{2\sqrt{\delta(1-\delta)}}\right), \tag{7.3}$$

so that for large k or σ the dense limit of large-scale upper-layer streets ($C \sim \delta$) is reached. As a general rule the propagation speed of hetonic streets increases with increasing aspect ratios, starting from zero for small k and reaching the sheet limit for large k without having a local maximum as long as the stratification parameter σ is small, i.e. as long as many vortices are located within one Rossby radius. In this case only a sheet-like mean behaviour can be expected. For larger stratification parameters, i.e. for a Rossby radius smaller than the typical distances between vortices, vortices basically 'feel' the nearest neighbours and the propagation speed C of symmetric hetonic streets is governed by the dilute approximation and becomes non-monotonic with a maximum for some finite aspect ratio k_{max} (compare upper solid curve in figure 10*a*). Figures 10(*b*) and 10(*d*) show the propagation speed C as a function of σ. The dashed curves in plot (*b*) representing the maximum speed which can be reached by symmetric hetonic streets for a given σ again show a non-monotonic behaviour: for small σ the maximum is the speed of sheets – when σ passes a critical value the maximum speed of pair-like streets (small k) becomes larger.

For $\epsilon \neq 0$ the dispersion relation can be solved only implicitly as for upper-layer streets. In the equivalent barotropic limit hetonic and upper-layer streets move with the same speed. In the barotropic limit hetonic streets stop moving.

One can derive upper and lower bounds for the critical aspect ratios

$$0 \leqslant k_{max} \leqslant \left(\frac{\xi_0^3 K_1(\xi_0)}{\pi}\right)^{1/3} \delta^{-1/3}\,\epsilon^{-1/3}, \tag{7.4}$$

using the corresponding inequalities (6.7)–(6.9) for upper-layer streets. The critical minimum aspect ratio of dilute antisymmetric hetonic streets can be estimated by

$$\frac{\pi}{32\xi_0^3 K_1(\xi_0)}\,\delta^{-1}\epsilon \leqslant k_{min}. \tag{7.5}$$

For decreasing stratification k_{min} increases and k_{max} decreases till they meet for some critical minimum stratification (σ_{min}) and only one solution can be found. A new basic feature of hetonic streets is that no antisymmetric streets can exist if the stratification

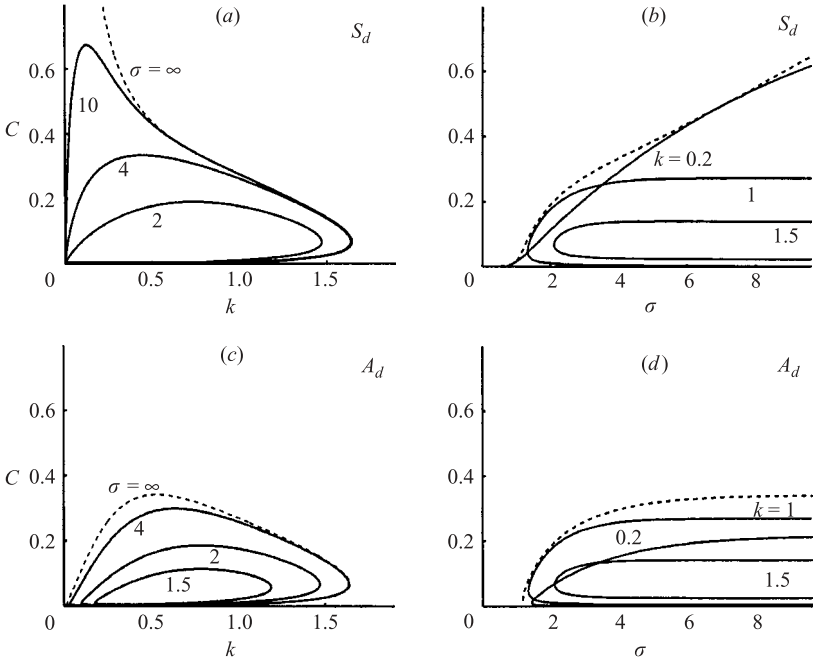

FIGURE 11. Same as figure 10 but for $\epsilon = 0.1$. The dashed lines in (b) and (d) represent the speed C_{max} at which the fastest symmetric or antisymmetric street can move for a given σ.

is below this critical value ($\sigma < \sigma_{min}$). The critical maximum aspect ratio of dense ($k \gg 1$) symmetric and antisymmetric hetonic streets can be estimated from

$$0 \leqslant k_{max} \leqslant \frac{2}{\mathrm{e}}\,\delta^{1/2}\epsilon^{-1/2}. \tag{7.6}$$

As can be seen from figures 11(a) and 11(c) the qualitative features remain basically the same as for upper-layer streets (figure 8a, c). Symmetric hetonic streets only exist if the aspect ratio is below some critical value k_{max}. For antisymmetric streets there is in addition a minimum critical aspect ratio k_{min}. In the non-critical domain, again always a fast and a slow vortex street exist. The solution curves for hetonic streets are all located below the equivalent baroclinic limit, which itself is the lower bound for upper-layer streets. So propagation speeds are always lower and the domain of existence grows with increasing stratification σ, unlike upper-layer streets. This can also be seen from figures 12(a) and 12(c) where ϵ_{crit} always decreases with decreasing stratification for fixed aspect ratio. The maximum critical planetary vorticity gradient reached for the equivalent barotropic limit is at the same time the minimum critical planetary vorticity gradient for the corresponding upper-layer streets (figures 9a and 9c). Depending on the aspect ratio k the propagation speed C changes differently with varying stratification σ (figures 11b and 11d). For small σ only pair-like symmetric streets exist (plot b). The maximum speed (dashed curve) of both solution branches is very small. For intermediate stratifications more sheet-like streets start to exist and move faster than pair-like symmetric streets. Further to the right pair-like symmetric streets move fastest. For antisymmetric hetonic streets plot (d) shows clearly the occurrence of a critical minimum stratification σ_{min} below which no quasi-stationary solutions can be found. As can be seen from figures 12(b) and 12(d) the domain of existence in the $k-\epsilon$ plane of hetonic streets depends strongly on stratification. There is

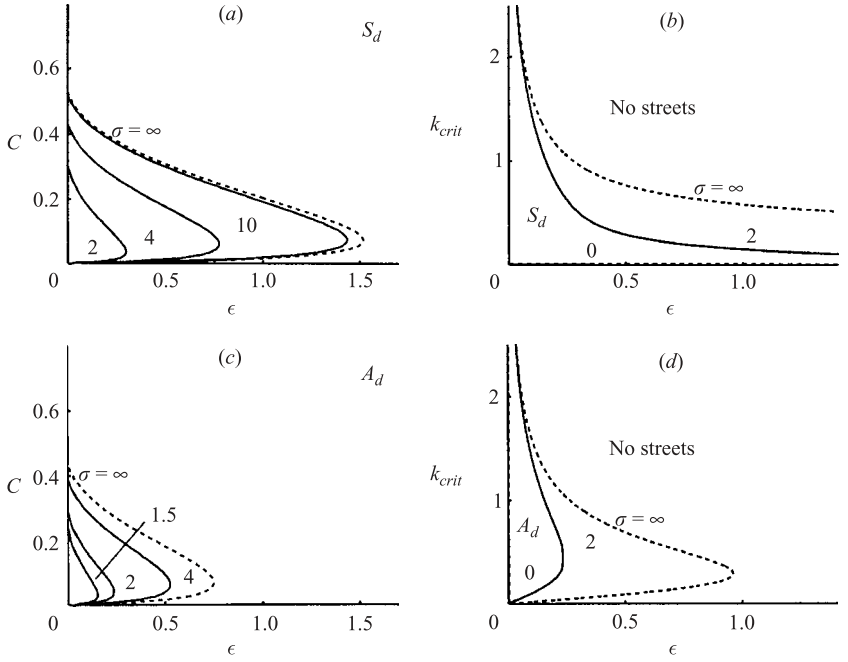

FIGURE 12. Same as figure 9 but for hetonic streets.

no essential difference with the corresponding curves of upper-layer streets in figure 9 except that the domains of existence are below the equivalent barotropic limit and that there is no finite barotropic limit.

Explicit asymptotic expressions for the propagation speed, the critical aspect ratios and the critical stratifications can again only be found in the limit of dense ($k \gg 1$) and dilute ($k \ll 1$) vortex streets.

The nearest neighbour approach for dilute ($k \ll 1$) symmetric vortex streets gives the expression for upper-layer streets with the second term again multiplied by the factor $-\delta/(1-\delta)$. Fast hetonic symmetric streets move under the additional assumptions $k\sqrt{\epsilon/C} \ll 1$ and $\epsilon/C \ll \sigma^2/(4\delta(1-\delta))$ with the speed (6.10) where C_f is now the propagation speed of symmetric dilute hetonic streets for $\epsilon = 0$. The correction of the f-plane speed of hetonic streets is the same as for upper-layer streets (6.10) and, up to a factor δ, also as for barotropic streets (5.4). It is always negative and follows for $\epsilon \ll k^2/(4C_f)$ an $\epsilon \ln(1/\epsilon)$ law, where C_f is the corresponding unperturbed f-plane speed.

Assuming now only small stratifications $\epsilon/C \gg \sigma^2/(4\delta(1-\delta))$ the dispersion relation of dilute symmetric streets can be reduced to

$$C = \frac{\sigma^2}{8\pi(1-\delta)} \sqrt{\frac{C}{\epsilon}}\, K_0\left(k\sqrt{\frac{\epsilon}{C}}\right). \tag{7.7}$$

This equation has no solutions if the stratification σ is above some critical minimum stratification σ_{min}. A lower bound can be given by

$$\sigma_{min} \geqslant \sqrt{\frac{8\pi}{\xi_0 K_0(\xi_0)}}\,(1-\delta)^{1/2}\,\epsilon^{1/2}\,k^{1/2} \;\approx\; 7.34\,(1-\delta)^{1/2}\,\epsilon^{1/2}\,k^{1/2}, \tag{7.8}$$

where for $\xi_0 \approx 0.47$ the function $\xi K_0(\xi)$ takes its maximum value ($\xi = k\sqrt{\epsilon/C}$). Equivalently equation (7.7) is only solvable for aspect ratios below the critical maximum aspect ratio k_{max}, which is bounded by

$$k_{max} \leqslant 0.02\,\sigma^2\,(1-\delta)^{-1}\,\epsilon^{-1}. \tag{7.9}$$

For small stratifications the barotropic behaviour of dilute symmetric streets is changed from the slow $\epsilon^{-1/3}$ to the faster ϵ^{-1} law (compare the solid curve in figure 12*b*). For small arguments $k\sqrt{\epsilon/C} \ll 1$ equation (7.7) yields

$$C = \frac{1}{64\pi^2}(1-\delta)^{-2}\epsilon^{-1}\sigma^4, \tag{7.10}$$

so that the propagation speed of dilute hetonic vortex streets increases only very slowly for small stratifications ($\sim\sigma^4$). This behaviour and the critical minimum stratification can best be seen in figure 11(*b*) for the curve corresponding to the aspect ratio $k = 0.2$. For large stratifications the propagations speed follows basically the corresponding f-plane curve represented in figure 10(*b*). Starting from the representation (7.7) of dilute hetonic streets the propagation speed of slow streets ($k\sqrt{\epsilon/C} \gg 1$) can be deduced:

$$C = k\epsilon^2 \ln^{-2}\left(\frac{\sigma^2}{8\sqrt{2\pi}(1-\delta)k\epsilon}\right). \tag{7.11}$$

This formula ceases to be valid for large stratifications.

Taking into account the influence of the nearest neighbours only, the dispersion relation for dilute antisymmetric streets ($k \ll 1$ and $\sqrt{\epsilon/C} \gg 1$) yields for $\sigma/\sqrt{4\delta(1-\delta)} \ll \sqrt{\epsilon/C}$ an estimation for the lower bound of the critical minimum stratification:

$$\sigma_{min} \geqslant \sqrt{\frac{\pi}{\max\{\xi^2 K_0(\xi)\}}}(1-\delta)^{1/2}\epsilon^{1/2}k^{-1/2} \approx 2.55(1-\delta)^{1/2}\epsilon^{1/2}k^{-1/2}, \tag{7.12}$$

where the maximum is reached for $\xi_0 \approx 1.55$ ($\xi = \sqrt{\epsilon/4C}$). Unlike symmetric dilute streets (see (7.8)) the critical minimum stratification increases with decreasing aspect ratios so that the zero stratification limit can never be reached by antisymmetric dilute streets (see curve for $k = 0.2$ in figure 11*d*). Through a transformation of equation (7.12) an estimation of the critical minimum aspect ratio k_{min} can be deduced:

$$k_{min} \geqslant 6.52\sigma^{-2}(1-\delta)\epsilon. \tag{7.13}$$

It shows the same linear ϵ behaviour as the barotropic limit (7.5) but with a stratification-dependent gradient following a σ^{-2} law. The joint effects of an infinite vortex row is, as for upper layer streets, already well approximated for aspect ratios $k > 1$. The propagation speed of fast dense hetonic streets ($k\sqrt{\epsilon/C} \ll 1$) can be approximated by (6.13) under the additional assumption $\sqrt{\epsilon/C} \ll \sigma/(2\sqrt{\delta(1-\delta)})$ where C_f is the propagation speed of dense hetonic streets on the f-plane. The first-order correction term is identical to that for dense upper-layer streets (6.13). It is negative and for $\epsilon \ll 1$ follows a $\sqrt{\epsilon}$ law. The curve for $k = 1$ on plots (*b*) and (*d*) of figure 4 can be seen as an illustration of this law. The other curves in the corresponding plots of figures 9 and 12 show a more complex behaviour which is between the square root and the logarithmic law of dilute streets.

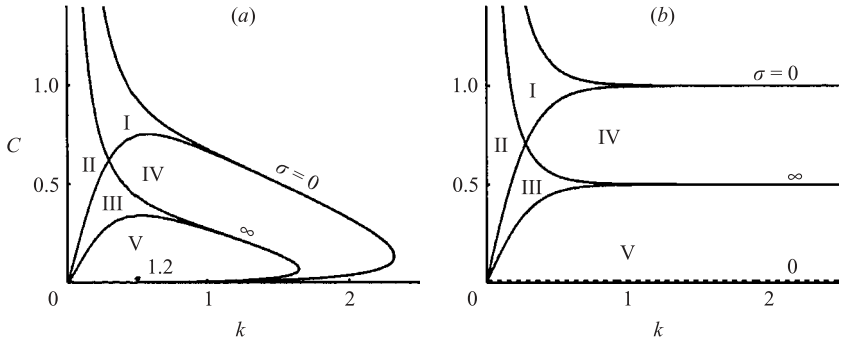

FIGURE 13. Domains I–V of existence of stratified vortex streets in the (C,k)-plane for (a) $\epsilon = 0.1$ and (b) $\epsilon = 0$, $\delta = 0.5$ on both plots. I: symmetric upper-layer streets; II: hetonic symmetric streets; III: symmetric hetonic and antisymmetric upper-layer streets; IV: symmetric and antisymmetric upper-layer streets; V: hetonic symmetric and antisymmetric streets.

Small stratifications $\sigma/(2\sqrt{\delta(1-\delta)}) \ll \sqrt{\epsilon/C}$ change the situation and the dispersion relation is given by

$$C = \frac{\sigma k}{8(1-\delta)} \sqrt{\frac{C}{\epsilon}} \exp\left(-k\sqrt{\frac{\epsilon}{C}}\right). \tag{7.14}$$

As for dilute hetonic streets no solution can be found if the stratification is below some minimum value. A lower bound for the critical minimum stratification σ_{min} is given by

$$\sigma_{min} \geqslant \sqrt{8\mathrm{e}}\,(1-\delta)^{1/2}\,\epsilon^{1/2}. \tag{7.15}$$

In (9.7) below the constraint (7.15) on σ is reformulated as a constraint on the vorticity density κ/a of a dense hetonic vortex street. For small stratifications only symmetric dilute hetonic streets can survive and for antisymmetric hetonic streets there exists a global minimum stratification (see figure 11d) which is due to the $k^{-1/2}$ behaviour of the lower bound of σ_{min} of antisymmetric dilute streets (see estimation (7.12)).

Thus we conclude that the simultaneous vertical and horizonal separation of vortices in hetonic streets generates a specific baroclinic dynamical behaviour which essentially differs from that of upper-layer streets.

8. Diagram of states

The analysis of the nonlinear dispersion relations (5.1), (6.1) and (7.1) for the different types of von Kármán streets is completed by a classification of possible states on a diagram of states on the (k, C)-plane with ϵ as the classification parameter. Figure 13(a) represents the diagram of states for $\epsilon = 0.1$, corresponding to the value used in the figures in previous sections. Five domains can be distinguished (see figure 13 for their definition). None of the five domains can reach arbitrary large aspect ratios. Domains III, IV and V can in addition never reach arbitrary small aspect ratios. Moreover area V, containing antisymmetric hetonic streets, cannot be found for stratifications $\sigma \leqslant \sigma_{min}(\epsilon)$. Figures 13 and 14 show how the classification diagram changes with changing ϵ. Figure 13(b) represents the case for $\epsilon \to 0$. Figure 14 shows changes with increasing ϵ. Figure 14(a) corresponds to the same topological class as the diagram of figure 13(a) but was calculated for $\epsilon = 0.85$, so that regions III, IV and V are clearly separated from the area of small aspect ratios. Depending on ϵ,

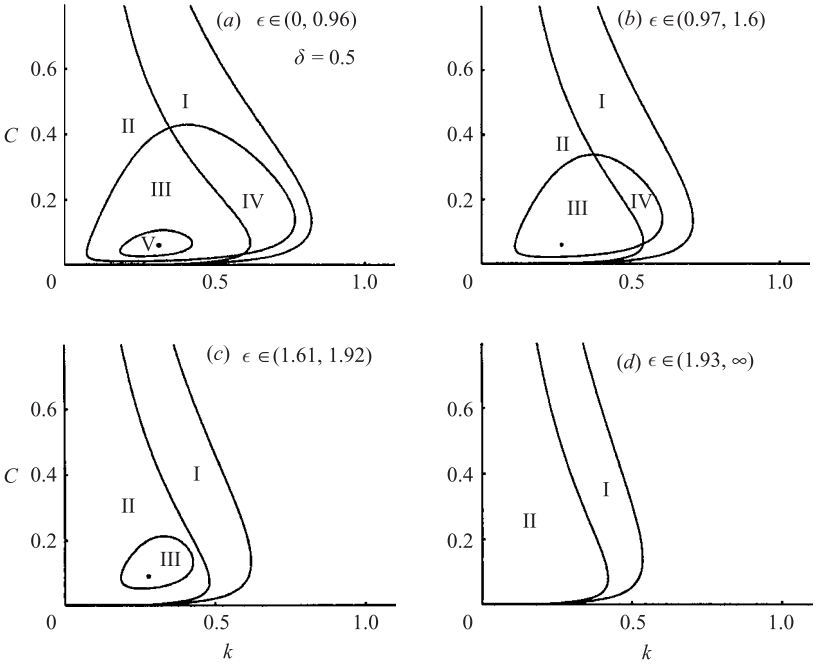

FIGURE 14. Representative diagrams of states for different intervals of planetary vorticity gradients ϵ; $\delta = 0.5$. In each interval the topology of the diagram of state remains the same. Notation is as in figure 13.

four different topological classes can be distinguished. Apart from the first class (plot *a*) for $\epsilon \in (0, 0.96]$, where all five regions are present and hetonic antisymmetric streets only exist if the stratification is above some critical value $\sigma_{min}(\epsilon)$ (here $\sigma_{min}(\epsilon) \sim 7.13$), a second class arises (plot *b*) for $\epsilon \in [0.97, 1.6]$, where region V vanishes so that no antisymmetric hetonic streets can be found and antisymmetric upper-layer streets only can survive if $\sigma \leqslant \sigma_{max}(\epsilon)$ (here $\sigma_{max} \approx 5.62$). In the interval $\epsilon \in [1.61, 1.92]$ (plot *c*) mixed domain IV vanishes. The critical maximum stratification for streets still exists and has decreased in the case represented to $\sigma_{max} \approx 2.19$. Finally if ϵ passes the critical threshold of 1.92 (plot *d*) region III also disappears and only symmetric streets can survive.

The diagram of states considered represents only a part of the full diagram of states of possible motions. On the beta-plane they are complemented in the sector $C < 0$ by Rossby waves. On the f-plane in the sector $C < 0$ there are vortex street solutions, obtained by changing the vorticity $\kappa \to -\kappa$, which corresponds to a reflection of figure 13(*b*) about the k-axis.

9. Characteristic scales of QG vortex streets

9.1. *Critical values*

In real geophysical flows QG vortex streets often represent the large-scale coherent part of turbulent QG beta-plane flows. The meridional size of such flows, e.g. zonal jets, will be limited by the maximally allowed meridional scale of the coherent structure (see for example the flow shown in figure 2).

Critical width. Expressions for the critical width of von Kármán streets can be obtained by reformulating in dimensional form the relations for the critical aspect ratios k. If the vortex strength κ and the separation a of vortices within one row is limited and β is given, the width of vortex streets cannot exceed a maximum value b_{max}. For dilute symmetric vortex streets ($a \gg b$) equation (5.3) leads to the dimensional expression

$$b_{max} = \left(\frac{\xi_{max}}{2\pi}\right)\left(\frac{\kappa}{\beta}\right)^{1/3} \approx 0.57\left(\frac{\kappa}{\beta}\right)^{1/3}. \tag{9.1}$$

This relationship shows that the critical width of vortex streets which are governed basically by pair interactions between vortices scales as $\beta^{-1/3}$ with the vortex strength κ as the relevant dynamical quantity. For dense symmetric and antisymmetric vortex streets ($b \gg a$) the dimensional form of (5.6) gives

$$b_{max} = \frac{2}{\mathrm{e}}\left(\frac{V}{\beta}\right)^{1/2} \approx 0.74\left(\frac{V}{\beta}\right)^{1/2}, \tag{9.2}$$

where $V = \kappa/2a$. The critical width of vortex streets governed by the mean interactions of many vortices scales as $\beta^{-1/2}$ with the vorticity density κ/a as the dynamical relevant quantity.

For antisymmetric streets there is at the same time also a critical minimum width, which in the dilute approximation ($a \gg b$) can be estimated from (5.8) to be

$$b_{min} = 0.17\,\frac{\beta a^4}{\kappa}. \tag{9.3}$$

Stratification effects on critical width. Stratification has a strong influence on the critical width and reduces the possible distances between vortices. Taking equations (6.7) for dilute ($a \gg b$) and (6.9) for dense ($a \ll b$) symmetric upper-layer streets one obtains

$$\delta^{1/3} b_\beta \leqslant b_{max} \leqslant b_\beta, \quad \delta^{1/2} b_\beta \leqslant b_{max} \leqslant b_\beta \tag{9.4}$$

respectively, with b_β the maximum barotropic distance given in equations (9.1) and (9.2). Since $\delta < 1$ the influence of stratification is felt more strongly by dense (sheet-like) streets, than by dilute (pair-like) streets. For hetonic streets using (7.4) and (7.6) one obtains

$$0 \leqslant b_{max} \leqslant \delta^{1/3} b_\beta, \quad 0 \leqslant b_{max} \leqslant \delta^{1/2} b_\beta \tag{9.5}$$

in the dense and dilute limit respectively. The lower bound for the critical maximum width of upper-layer streets is at the same time the upper bound for hetonic streets. The lower bound for the critical maximum width of hetonic streets is zero.

Critical vorticity strength and density. All formulae for the critical width and critical zonal distance can be transformed to expressions for the critical minimum vortex strength. For example barotropic antisymmetric streets can only be found if

$$\kappa \geqslant \kappa_{min} \quad \text{with} \quad \kappa_{min} = \frac{2}{\epsilon_{max}}\,\beta\, a^3 \approx 1.04\,\beta\, a^3 \tag{9.6}$$

or dense ($a \ll b$) hetonic streets if

$$V \geqslant V_{min} \quad \text{with} \quad V_{min} = \mathrm{e}\,\beta\, R^2. \tag{9.7}$$

If the geometry, vortex strength and planetary vorticity gradient are prescribed (9.7) yields an upper bound for the Rossby radius R, i.e. critical stratification.

Critical planetary vorticity gradient. If on the other hand the vortex strength κ and the geometry of a street are fixed there can only be a solution if β is below some critical value β_{max} or equivalently, if the street is located above some critical latitude ϕ_{min} when beta is treated as the planetary vorticity gradient on the sphere ($\beta = 2\Omega/R_p \sin\Phi$). From this it follows that antisymmetric vortex street-like global flows will only be found in latitudes not too close to the equator of a rotating planet. Since for given planetary rotational frequency Ω the vorticity gradient β decreases with increasing planetary radius R_p vortex-street-like global flows will exist for a wider range of parameters on larger planets than on smaller ones. Both results seem to be in agreement with observations of vortex structures on Jupiter (Ingersoll 1990 and Marcus & Lee 1994). However, we emphasize that this result does not take into account the effect of background shear flows on vortex dynamics, although this effect can be significant, see e.g. Youssef & Marcus (2003).

Critical zonal distance. The maximum planetary vorticity gradient $\epsilon_{max} \sim 1.92$ beyond which no barotropic antisymmetric street can exist (see figure 5) gives a dimensional relation for the maximum separation a_{max} of vortices in one row:

$$a_{max} = \left(\frac{\epsilon_{max}}{2}\right)^{1/3} \left(\frac{\kappa}{\beta}\right)^{1/3} = (\epsilon_{max})^{1/2} \left(\frac{V}{\beta}\right)^{1/2}. \tag{9.8}$$

The typical velocity of the flows produced by von Kármán streets is given by $V = (\bar{u}_{max} - \bar{u}_{min})/2$, which corresponds to half the velocity jump of the zonal mean flow, i.e. the difference of the maximum and minimum speed of the mean flow.

9.2. *Estimations for laboratory and numerical experiments and natural conditions*

The diagram of states for antisymmetric barotropic streets shown in figure 5 can be compared to the diagram of states (figure 1*c*) in Flierl *et al.* (1987) obtained by their numerical simulations of antisymmetric vortex streets arising from a perturbed zonal jet with Gaussian velocity profile on an doubly periodic barotropic beta-plane. They calibrated their model to conditions typical for the Gulf Stream, using as scales the half-width $l = 100\,\mathrm{km}$ and maximum speed $U_{max} = 2\,\mathrm{m\,s^{-1}}$ of the jet. The direction of propagation of streets is in agreement with our theory ($c > 0$). In the range of parameters covered in numerical runs they found the existence of a critical maximum planetary vorticity gradient $\beta^\star = \beta l^2/U_{max} = 0.5$, beyond which vortex streets cease to exist and a transition to a different flow regime occurs. This value is defined with accuracy (± 0.2) due to the limited number of experiments. Our theory describes this transition, see the solid line in figure 5, where the critical maximum planetary vorticity gradient $\beta^\star$ corresponds to $\epsilon_{max} = 1.92$. To compare the numerical and theoretical results formula (9.8) can be used to derive the zonal distance between vortices a_{max}. If we identify the distance b between vortex rows with l, our characteristic velocity V with U_{max} and assume $\beta^* = 0.414$ in accordance with data we obtain the theoretical estimation $a_{max} \approx 2.2\,l = 220\,\mathrm{km}$. The maximum distance between vortices along the row of the corresponding numerical vortex street, with $k^\star = 1.227$, is $a_{max} = 360\,\mathrm{km}$. This result does not take into account finite core effects and thus underestimates the maximum distance.

Both diagrams show an increase of the interval of existence for decreasing planetary vorticity gradients. However a detailed comparison between the numerically and theoretically derived relationships for the increase is again impossible, since from the limited number of numerical runs only roughly interpolated curves are available.

	δ	σ	β ($m^{-1}\,s^{-1}$)	$2V$ ($m\,s^{-1}$)	a_{crit}(m)	b_{crit}(m)
Ocean ($R=\infty$)	0.2	0	1.15×10^{-11}	0.25	140×10^3	42×10^3
Ocean ($R=0$)	0.2	∞	1.15×10^{-11}	0.25	77×10^3	19×10^3
Atmosphere ($R=\infty$)	0.5	0	1.15×10^{-11}	10	900×10^3	270×10^3
Atmosphere ($R=0$)	0.5	∞	1.15×10^{-11}	10	775×10^3	190×10^3
Jupiter ($R=\infty$)	1	0	10^{-12}	50	4900×10^3	1420×10^3
Small tank ($R=\infty$)	1	0	26	0.2	0.1	0.03
Coriolis ($R=\infty$)	1	0	0.02	0.05	1.55	0.45

TABLE 1. Critical geometry of antisymmetric streets in different typical situations. The barotropic case ($R=\infty$) is the upper limit, where stratification effects are not felt. The lower limit is represented by the equivalent barotropic case ($R=0$). The critical widths based on symmetric vortex streets are in general larger, twice as big for example in the two cases given for the ocean. On Earth and Jupiter a reference latitude of 60° is chosen.

The generalization to different baroclinic cases is described by the diagrams of states for upper-layer and hetonic streets (see plots (*b*) and (*d*) of figures 9 and 12). Taking ϵ_{max} from these diagrams and using as before equation (9.8) the critical scales of vortex streets can be estimated for typical atmospheric, oceanic, jovian and laboratory conditions (for a summary see table 1).

For the ocean a typical midlatitude situation ($\approx 60°$) in the Southern Ocean is chosen. There we have the planetary vorticity gradient $\beta = 1.15\times10^{-11}\,m^{-1}\,s^{-1}$, a relative thickness of the upper layer of $\delta = 0.2$ and a Rossby radius of $R = 10$ km. As a basis for the estimations a zonal flow with a velocity jump of $2V = \overline{u}_{max} - \overline{u}_{min} = 0.25\ m\,s^{-1}$ is considered. Assuming that the distances between vortices are much smaller than the Rossby radius ($\sigma = 0$) we find $a_{max} = 140$ km as the maximum distance between vortices in the x-direction and a corresponding street width of $b_{max} = 42$ km. Since the distances are larger than the Rossby radius these critical distances are only an upper bound. The lower bound for the critical horizontal scales is obtained assuming that distances between the vortices are much larger than the Rossby radius ($\sigma = \infty$). They are $a_{max} = 77$ km in the x-direction and $b_{max} = 19$ km in the y-direction. The real values are in between since $2 \leqslant \sigma \leqslant 5$. Going to the sheet limit $a \ll b$, the critical width increases. As upper bound one has $b_{max} = 77$ km and as lower bound $b_{max} = 34$ km.

So in the Southern Ocean at 60° south the critical width of the central part (distance between inflection points) of intermittent zonal flows induced by von Kármán streets is in all cases roughly of the order of the Rossby radius. Intermittent flows induced by hetonic vortex streets have smaller horizontal scales than the intermittent flows induced by upper-layer vortex streets. The lower bounds for the jet-like flows induced by upper-layer vortex streets are upper bounds for front-like flows induced by hetonic vortex streets, so that the critical widths of the mean flows induced by hetonic vortex streets are also comparable to the Rossby radius.

The fact that for a given speed of the mean flow induced by a vortex street the width is limited gives a good explanation for the multi-jet-structure of the Antarctic Circumpolar Current, assuming that the oceanic flow self-organizes into vortex streets. If we assume that a jet is roughly four times wider than its central part we find distances from one jet to the next of between 120 km and 240 km, which is in agreement with the values gathered from observations.

For atmospheric flows $\beta = 1.15 \times 10^{-11}\,\mathrm{m^{-1}\,s^{-1}}$, equal layers $\delta = 0.5$ and a baroclinic Rossby radius of 700 km are assumed. Taking zonal mean flows with a typical velocity jump of $\overline{u}_{max} - \overline{u}_{min} = 10\,\mathrm{m\,s^{-1}}$ one obtains $a_{max} = 900$ km as upper bound for the maximum distance in the x-direction and $b_{max} = 775$ km in the y-direction. The lower bound is given by $a_{max} = 775$ km and $b_{max} = 190$ km. The real value again lies somewhere in between. Since we have taken the same planetary vorticity gradient for the atmosphere and ocean, the typical horizontal critical scales of atmospheric vortex streets are larger by a factor of $\sqrt{V_{atmos}/V_{ocean}} \approx 6.3$ in the barotropic limit.

On Jupiter at 60° latitude β is about $10^{-12}\,\mathrm{m^{-1}\,s^{-1}}$ and the typical velocity jump of the zonal mean flow systems in the visible cloud layer is roughly $50\,\mathrm{m\,s^{-1}}$ so that the critical horizontal scales for vortex streets in the barotropic limit are 7 times larger on Jupiter than in the terrestrial atmosphere which is again in agreement with the horizontal scales of the periodic vortex structures observed.

The experimental set-up of e.g. Sommeria, Meyers & Swinney (1991) has a rotational period of $T_{tank} = 0.2$ s. The bottom slope ($s_b = 0.1$) introduces, with the mean fluid depth $h_0 = 0.2$ m, a topographic vorticity gradient $\beta \approx 26\,\mathrm{m^{-1}\,s^{-1}}$. If one assumes further a typical velocity jump $\overline{u}_{max} - \overline{u}_{min} = 0.2\,\mathrm{m\,s^{-1}}$ of the mean flow, the vortex centres cannot exceed the separation $a_{max} \approx 0.1$ m and the corresponding width should be $b_{max} \approx 0.03$ m. In the dense limit ($a \ll b$) equation (9.2) gives the critical distance between the vortex rows (sheet) of $b_{max} = 0.05$ m. It seems that in this fast-rotating small tank the dimensions of the vortex streets are at the limit of the resolving power of the device.

A typical experimental set-up of a vortex experiment with the largest rotating tank available at present (Coriolis, France) has a rotational period of the tank of $T_{tank} = 50$ s. With a bottom slope gradient of $s_b = 0.05$, a mean fluid depth of $h_0 = 0.5$ m, we obtain a topographic vorticity gradient of $\beta = 0.02\,\mathrm{m^{-1}\,s^{-1}}$. Assuming a velocity jump of $\overline{u}_{max} - \overline{u}_{min} = 0.05\,\mathrm{m\,s^{-1}}$ the maximum distance between vortices in one row is given by $a_{max} = 1.55$ m and the corresponding width $b_{max} = 0.45$ m. If we consider the critical width in the sheet limit ($a \ll b$) using (9.2) we find as critical maximum width $b_{max} = 0.82$ m, so that vortex street phenomena on the beta-plane should be resolvable using the Coriolis tank. The theory of symmetric vortex streets can be used to describe currents induced by a row of vortices along a boundary with a sloping bottom. Of course the estimations are only very rough since curvature effects of the annulus as well as forcing and dissipation effects are not accounted for by the theory.

10. Region of applicability and discussion

In this section it will be shown to what extent the results of the QG two-layer theory of von Kármán vortex streets depends on the horizontal and vertical structure of the PV field, the specific profile of background stratification, the nonlinear curvature effects on planetary scales and finally on the effects of interaction with ambient shear flows and Rossby waves.

10.1. *Vertical structure of PV localization and continuous stratification effects*

In the two-layer model QG PV anomalies associated with a single vortex are of finite vertical extent and are distributed uniformly within each layer, which is a special limiting case of three-dimensional PV distributions in continuously stratified fluids. A complementary limiting case corresponding to localized modified PV anomalies of

very thin vertical extent (Flierl 1987; Gryanik 1988) is described by

$$Q=\gamma\sum_{m=-\infty}^{\infty}\left[\delta(x-ma)\delta\left(y-\tfrac{1}{2}b\right)\delta(z-z^{+})-\delta(x+s-ma)\delta\left(y+\tfrac{1}{2}b\right)\delta(z-z^{-})\right], \quad (10.1)$$

with γ the vortex strength (three-dimensional analogue of κ), s the shift of the rows, and $z^{\pm}$ the vertical vortex coordinates of cyclones (+) and anticyclones (−).

As has been shown in § 2.2 all aspects of QG von Kármán vortex street theory are determined by the corresponding Green's function, so that the universality of the results gained from a two-layer model can be judged from a comparison with the Green's functions of continuously stratified models. Although the exact structure of the Green's function in stratified fluids obviously depends on the profiles of the Brunt–Väisälä frequency at large scales ($r\gg R_0$) the Green's function always has universal barotropic asymptotics and is thus insensitive to the details of the stratification profiles. In continuously stratified fluids the effect of finite R_0 at scales $r\sim R_0$ is described by a two-mode approximation (barotropic and first baroclinic) which is equivalent to the two-layer approximation (see e.g. Gryanik *et al.* 2000). This approximation neglects the vortex interactions due to higher-order baroclinic modes, which become important at small separations r between vortices, and hence differences between two-layer and continuously stratified models arise at small scales ($r\ll R_0$). We can easily quantify this difference, since in the limit of small scales arbitrary stratification profiles can be approximated by a profile of constant Brunt–Väisälä frequency N and since the Green's function for fluids between two horizontal flat boundaries can be given explicitly in this case, see Appendix C. Using the Green's function (C 1), (C 2) and retracing the procedure of derivation of the nonlinear dispersion relation described in § 2.2 we find

$$c=\frac{\gamma Nb}{4\pi f}\sum_{n=-\infty}^{\infty}\sum_{m=-\infty}^{\infty}\left[\left(1+\frac{1}{r_{nm}^{-}}\right)\frac{\exp(-\lambda r_{nm}^{-})}{r_{nm}^{-}}+\left(1+\frac{1}{r_{nm}^{+}}\right)\frac{\exp(-\lambda r_{nm}^{+})}{r_{nm}^{+}}\right], \quad (10.2)$$

where $\lambda=\sqrt{\beta/c}$ and $r_{mn}^{\pm}=[(ma-s)^2+b^2+\frac{N^2}{f^2}(d^{\pm}-2Hn)^2]^{1/2}$ are the three-dimensional distance functions with the shift between rows $s=0$ for symmetric streets and $s=a/2$ for antisymmetric streets and the vertical distances $d^{-}=z_{+}-z_{-}$ between vortices and $d^{+}=z_{+}+z_{-}$ between vortices and first vertical images. A systematic and detailed analysis (similar to that given in §§ 5 to 7) will form part of future studies. The limit of dilute streets of equation (10.2), coinciding with vortex pairs and vortex tripoles, was investigated for infinite and semi-infinite layer depths by Flierl (1987) and Gryanik (1988). From these studies it follows that the speed of propagation of QG von Kármán vortex streets at small scales depends on the degree of vertical localization of the PV field (column-like vortices in the two-layer model and blob-like vortices in continuously stratified models). At small scales ($r\ll(N/f)d^{-}$) the azimuthal velocity v of an individual column-like vortex is $v\sim r\ln r$ in a two-layer model instead of $v\sim r$ for a blob-like vortex in a continuously stratified model. The interaction between vortices in a continuously stratified fluid increases in the limit of small distances since more and more higher-order baroclinic modes come into play. Correspondingly for small scales, the region of existence and the speed of propagation of streets increases, even more strongly than in the case of a two-layer fluid.

10.2. *Surface boundary condition and 'compressibility' effects*

The rigid lid boundary conditions, used in our investigation, filter out the effect of superinertial waves and are natural at the bottom, and quite justified at the surface if

the typical size of the domain is much smaller than the barotropic Rossby–Obukhov deformation radius $L_0 = (gH)^{1/2}/f$. For oceanic conditions $L_0 \gg R_0$, so that the rigid lid boundary condition can be used. For the atmosphere on the other hand, the rigid lid condition is too restrictive. The analysis of Gryanik (1983) shows that in the case of a QG two-layer model with a finite barotropic deformation radius L_0 the interaction between vortices exponentially decreases for $r \gg L_0$ even without the β-effect, mainly due to the modification of the barotropic part of the Green's function. So, the propagation speed of QG von Kármán vortex streets becomes affected by compressibility at scales comparable with or larger than the barotropic deformation radius L_0.

It should be stressed that the non-existence of westward propagating vortex streets in the model under consideration is due to the rigid lid boundary condition. If the Rossby–Obukhov radius L_0 is taken to be finite, vortex streets can also exist, as long as the necessary condition $c < -\beta R_0^2$ is satisfied. Only under these condition can localized vortices propagating westward exist (see Nycander 1994). Although the condition $c < -\beta R_0^2$ is not very realistic for the ocean on Earth, it can be realized in the atmospheres of giant planets and in laboratory experiments. Quantitative results on the effects of a finite L_0 on the properties of QG von Kármán vortex streets can easily be obtained in the barotropic case by taking the dispersion relation (3.4) of barotropic vortex streets with the modified length scale $\lambda = \sqrt{\beta/c + 1/L_0}$. In particular, the analysis shows that $c \to -\beta L_0^2$ from below in the limit $\beta b^2/\kappa \to 1/L_0$. The speed c coincides with the critical speed $c_{Rossby} = -\beta L_0^2$ of barotropic Rossby waves reached from above. The case of a QG two-layer model with a finite L_0 needs an additional detailed analysis, especially in the velocity range $-\beta L_0 < c < 0$, where von Kármán vortex streets can interact with Rossby waves.

10.3. *Stability, Rossby wave radiation and shear effects*

QG vortex streets can become dynamically unstable due to perturbations of the positions of the individual vortices forming the street. The linear stability analysis of von Kármán streets in 1 1/2-layer models performed by Stewart (1945) and Masuda & Miki (1995) show that stratification increases the stability of von Kármán vortex streets with respect to streets in barotropic fluids. Finite cores of vortices also increases the stability region of vortex streets as was investigated by Saffman & Schatzman (1982). Also, horizontal boundaries stabilize vortex streets as shown in Rosenhead (1929). These different stabilization effects are expected to also be valid for two-layer QG von Kármán vortex streets. The instability analysis of QG von Kármán vortex streets is an attractive subject for future investigation, which will extend the previous work to the case of stratified and differentially rotating fluids.

It is necessary to bear in mind, however, that perturbations in the positions of individual vortices forming the street on the beta-plane are accompanied in general by Rossby wave radiation (Gryanik 1992*a*; Korotaev 1997), so that the radiation of Rossby waves by vortices can be an additional mechanism of instability of QG von Kármán vortex streets. We notice that the speed of propagation of QG von Kármán vortex streets $c > 0$ is outside the range of phase speed of Rossby waves $c < 0$, so the radiation of Rossby waves by the Cherenkhov mechanism by steady propagating QG von Kármán vortex streets without perturbations is impossible. To obtain a qualitative *a priori* insight into the physics of radiation of Rossby waves of QG von Kármán vortex streets, we can consider the limit of dilute streets and use the results of Reznik (1992) on the dynamics of an individual point vortex on the beta-plane. According to Reznik (1992), see also Reznik *et al.* (1997), cyclonic vortices

propagate to the north west, and anticyclonic ones to the south west. Obviously, this type of dynamics will increase the separation between the vortex rows of opposite sign forming the street, and so decrease the mutual interaction between vortices. Finally, we can expect a decreased eastward propagating speed of the vortex street. To what extent the combined effects of perturbation in position of vortices and of radiation of Rossby waves by vortices forming the street control the stability of the vortex streets is an open question.

Obviously, in real geophysical situations self-organization of turbulent zonal jets is accompanied by interaction processes with large-scale regular background flows. In the laboratory and numerical experiments of Marcus & Lee (1998) and Youssef & Marcus (2003) von-Kármán-type vortex structures propagating to the west are documented, in the case where cyclonic vortex chains are placed in the cyclonic flanks and anticyclonic vortex chains in the anticyclonic flanks of westward propagating barotropic background jets. We think that the difference with our results could be attributed to the presence of a non-uniform asymmetric background shear flow. The analytical analysis of the case of a constant baroclinic background shear flow in a two-layer beta-plane QG model (Borth 1999) also shows that the interaction with background shear flows modifies the solvability condition and diagram of states.

Summarizing, many factors can influence the results obtained with our idealized model and it is possible that also in the frame of the QG-model the set of exact solutions found can be incomplete. All this indicates that focused laboratory and numerical experimental studies are urgently needed to support or reject the theoretical predictions.

11. Conclusions

A theory of QG von Kármán streets in two-layer fluids on beta-plane has been developed.

The theory can be used to describe the large-scale anisotropic part of quasi-zonal turbulent flows arising naturally in oceanic (Rintoul, Hughes & Olbers 2000), atmospheric (Ingersoll 1990) and rotating tank flows (Sommeria *et al.* 1991) as well as in many different numerical models running under atmospheric, oceanic or more general planetary conditions such as on Jupiter (Wolff, Maier-Reimer & Olbers 1991; Marcus & Lee 1998; Rintoul *et al.* 2000 and references therein). The theory also provides qualitative knowledge about the topology and dynamics of non-QG flows, since the basic mechanism of self-organization of localized vortices into periodic structures is similar, see for example Pao, Lai & Schemm (1982). A qualitative description of self-organized vortex streets with a horizontal axis, which are a model of spiral symmetric vortex street solutions of the Boussinesq equations were suggested for atmospheric boundary layer vortices by Gryanik (1992*b*) and for acoustic gravity vortices in the stratosphere by Stenflo (1994).

We hope that the theory of QG von Kármán vortex streets will be useful for developing new models of balanced intermittent jets and fronts and for understanding other problems of geophysical fluid dynamics such as for example the passive scalar, chemical and biological transport in highly intermittent turbulent flows, in which the coherent part is important and can be represented by von-Kármán-type vortex streets. The modelling of intermittent jet-like or frontal zones by QG von Kármán streets can help to explain naturally the east–west anisotropy of jets, the existence of a critical width and stratification and allows dynamically based scalings to be introduced.

We are glad to thank S. Danilov, B. Galperin, V. Goncharov, D. Marshall, J. Marshall, G. Reznik, M. Sokolovskiy, S. Sukoriansky, G. Sutyrin, C. Völker and J.-O. Wolff for many helpful comments concerning the questions considered in this study. The work was partly supported by EC project CARTUM – Contract MAST3-CT98-0172 and a fellowship from Hanse Institute for Advanced Study. We thank Hanse Institute for Advanced Study for its kind hospitality.

Appendix A. Green's function representations

The explicit form of the streamfunction $\psi_A(x, y)$ of a vortex-induced flow is given by the Green's function of an individual vortex $G^{\lambda}_{\alpha}(x, y)$ (see equation (2.9)) summed over all positions of the vortices belonging to the vortex structure.

The condition of a-periodicity in the x-direction gives the possibility of introducing the explicit form of the appropriate Green's function corresponding to a vortex row $G^{\lambda}_{row}(x, y; x_0, y_0)$ by summing the contributions of the periodically spaced vortices. It is defined by

$$G^{\lambda}_{row}(x, y; x_0, y_0) = \sum_{m=-\infty}^{+\infty} G^{\lambda}(x - x_0 - ma, y - y_0). \tag{A 1}$$

The summation over Green's function G^0 is expressible in closed form as

$$G^{0}_{row}(x, y; x_0, y_0) = \frac{1}{4\pi} \ln\left(\cosh\frac{2\pi(y - y_0)}{a} - \cos\frac{2\pi(x - x_0)}{a}\right), \tag{A 2}$$

see e.g. Lamb (1932). In the case $\lambda \neq 0$ one has to calculate the sum (3.2). Although this sum converges rapidly, it cannot be written in closed analytical form. This representation of Green's function (A 1) emphasizes the contributions of individual point vortices to the total flow induced by the vortex row. A complementary representation for the Green's function of a vortex row emphasizing the integral effects of all vortices in the row can be found in a few steps. First we calculate the Fourier transform $\widehat{G}_{row}(\mathbf{k})$ of $G_{row}(\mathbf{r})$:

$$\widehat{G}^{\lambda}_{row}(\mathbf{k}) = -\frac{\mathrm{e}^{-\mathrm{i}k_x x_0 - \mathrm{i}k_y y_0}}{k_x^2 + k_y^2 + \lambda^2} \sum_{m=-\infty}^{\infty} \mathrm{e}^{-\mathrm{i}k_x am}, \tag{A 3}$$

where $\mathbf{k} = (k_x, k_y)$ is the wave vector. Next we substitute the sum of exponential functions using the Poisson summation formula

$$\sum_{m=-\infty}^{\infty} \mathrm{e}^{-\mathrm{i}k_x am} = \frac{2\pi}{a} \sum_{n=-\infty}^{\infty} \delta\left(k_x - \frac{\pi n}{a}\right) \tag{A 4}$$

and apply the inverse Fourier transform to $\hat{G}_{row}(\mathbf{k})$ by first integrating over k_x and then over k_y. Using the integration formula

$$\int_0^{\infty} \frac{\cos y k_y}{k_y^2 + \mu_n^2}\, \mathrm{d}k_y = \frac{\pi}{2\mu_n} \mathrm{e}^{-\mu_n |y|} \tag{A 5}$$

with $\mu_n^2 = \lambda^2 + (\pi n/a)^2$ (see Gradshteyn & Ryzhik 1979) gives the result (3.3).

Appendix B. Asymptotic expressions for the propagation speed

To calculate the asymptotical behaviour of the propagation speed for large $k = b/a$ (dense vortex streets) we will use the formulae for the velocity field of the row:

$$u(x, y) = \operatorname{sign}(y - y_0)\frac{1}{2a}\left[e^{-\lambda|y-y_0|} + 2\sum_{n=1}^{\infty} \exp(-\sqrt{(2\pi n/a)^2 + \lambda^2}|y - y_0|)\cos\frac{2\pi n}{a}(x - x_0)\right], \tag{B 1}$$

$$v(x, y) = \frac{2\pi}{a^2}\sum_{n=1}^{\infty} \frac{\exp(-\sqrt{(2\pi n/a)^2 + \lambda^2}|y - y_0|)}{\sqrt{(2\pi n/a)^2 + \lambda^2}} n \sin\frac{2\pi n}{a}(x - x_0). \tag{B 2}$$

We obtain the propagation speed c of a symmetric barotropic street by evaluating $\kappa\, u(0, b/2)$ for a vortex row shifted by $x_0 = 0$ and $y_0 = -b/2$:

$$c = \frac{\kappa}{2a}\left[e^{-\lambda b} + 2\sum_{n=1}^{\infty} \exp(-\sqrt{(2\pi n/a)^2 + \lambda^2}\, b)\right]. \tag{B 3}$$

The leading terms of the expansion for $a \ll 1/\lambda$ can be calculated in explicit form by keeping in the sum only terms depending on m and summing using the geometric progression formula. The result is

$$c = \frac{\kappa}{2a}\left[e^{-\lambda b} + 2(\exp(2\pi b/a) - 1)^{-1}\right]. \tag{B 4}$$

Similarly the propagation speed c of an antisymmetric barotropic street is obtained by evaluating $\kappa u(0, b/2)$ for a vortex row shifted by $x_0 = a/2$ and $y_0 = -b/2$:

$$c = \frac{\kappa}{2a}\left[e^{-\lambda b} + 2\sum_{n=1}^{\infty}(-1)^n \exp(-\sqrt{(2\pi n/a)^2 + \lambda^2}\, b)\right]. \tag{B 5}$$

The asymptotics in the limit $a \ll 1/\lambda$ is given by

$$c = \frac{\kappa}{2a}\left[e^{-\lambda b} - 2\left(e^{2\pi b/a} + 1\right)^{-1}\right]. \tag{B 6}$$

The asymptotic propagation speeds c for the other vortex streets S_e, A_e, S_d and A_d are obtained by taking the appropriate linear combinations of the asymptotic formula (B 4) and replacing λ by λ_1 and λ_2.

To calculate approximate formulae for the propagation speeds c for streets with aspect ratios $b/a \ll 1$ (dilute vortex streets) the first representation in terms of modified Bessel functions is more convenient.

Appendix C. Green's function for a continuously stratified fluid

The Green's function for a continuously stratified fluid with flat rigid boundaries is calculated easily by the method of images from the Green's function for an unbounded domain. The result of straightforward calculation is

$$G(r, z, z_0) = \sum_{n=-\infty}^{+\infty} \{G_0(r, z - z_0 + 2Hn) + G_0(r, z + z_0 + 2Hn)\}, \tag{C 1}$$

with

$$G_0(r,z) = -\frac{N}{4\pi f}\frac{\exp\left(-\lambda\left(r^2+\frac{N^2}{f^2}z^2\right)^{1/2}\right)}{(r^2+(N^2/f^2)z^2)^{1/2}}, \qquad (C\,2)$$

where $\lambda^2 = \beta/c$ as before and $G_0(r,z)$ is the Green's function in an unbounded fluid (Flierl 1987; Gryanik 1988).

REFERENCES

Aref, H. & Siggia, E. D. 1981 Evolution and breakdown of a vortex street in two dimensions. *J. Fluid Mech.* **109**, 435–463.

Barkley, R. A. 1968 The Kuroshio-Oyashio front as a compound vortex street. *J. Mar. Res.* **26**, 83–104.

Barkley, R. A. 1972 Johnston atoll's wake. *J. Mar. Res.* **30**, 201–216.

Bénard, H. 1908 Formation de centres de giration à l'arrière d'un obstacle en mouvement. *C. R. 'Acad. Sci. Paris* **148**, 839–842.

Borth, H. 1999 Von Kármánsche Wirbelstraßen und barokline Jetströme in einem 2-Schichten Kanal auf der beta-Ebene. PhD thesis, University of Bremen, Germany. (Available from Alfred-Wegener-Institut für Polar- und Meeresforschung. 1999 AWI Rep. 96, 147 pp.)

Borth, H, Gryanik, V. M., Olbers, D. J. & Wolff, J.-O. 2004 A von Kármán attractor in a quasi-geostrophic wind-driven two-layer turbulent channel flow. *In preparation.*

Burlaga, L. F. 1990 A Heliospheric vortex street. *J. Geophys. Res.* **95** (A4), 4333–4336.

Danilov, S. D., Gryanik, V. M. & Olbers, D. J. 2001 Equilibration and lateral spreading of a strip-shaped convective region. *J. Phys. Oceanogr.* **31**, 1075–1087.

Durgin, W. W. & Karlsson, S. K. F. 1971 On the phenomenon of vortex street breakdown. *J. Fluid Mech.* **48**, 507–527.

Etling, D. 1989 On atmospheric vortex streets in the wake of large islands. *Met. Atmos. Phys.* **41**, 157–164.

Fernandez, V. M., Zabusky, N. J. & Gryanik, V. M. 1995 Vortex intensification and collapse of the Lissajous-elliptic ring: single- and multi-filament Biot-Savart simulations and visiometrics. *J. Fluid Mech.* **299**, 289–331.

Flierl, G. R. 1987 Isolated eddy models in geophysics. *Annu. Rev. Fluid Mech.* **19**, 493–530.

Flierl, G. R., Malanotte-Rizzoli, P. & Zabusky, N. J. 1987 Non-linear waves and coherent vortex structures in barotropic β-plane jets. *J. Phys. Oceanogr.* **17**, 1408–1438.

Godfrey, D., Hunt, G. E. & Suomi, V. E. 1983 Some dynamical properties of vortex streets in Saturn's atmosphere from analysis of Voyager images. *Geophys. Res. Lett.* **9**, 865–868.

Gradshteyn, I. S. & Ryshik, I. M. 1979 *Table of Integrals, Series, and Products.* Academic.

Gryanik, V. M. 1983 Dynamics of singular geostrophic vortices in a two-layer model of the atmosphere (ocean). *Izv. Atmos. Ocean. Phys.* **19**, 227–240.

Gryanik, V. M. 1986 singular geostrophic vortices on the β-plane as a model for synoptic vortices. *Oceanology* **26**, 126–130.

Gryanik, V. M. 1988 Localized vortices – 'vortex charges' and 'vortex filaments' in a baroclinic differentially rotating fluid. *Izv. Atmos. Ocean Phys.* **24**, 919–926.

Gryanik, V. M. 1992*a*. Radiation of rossby waves and adaptation of potential vorticity fields in the atmosphere (ocean). *Trans. (Dok.) USSR Acad. Sci.* **326**(6), 976–979.

Gryanik, V. M. 1992*b*. Localized vortices and coherent vortex structures in the unstable boundary layer. *Trans. (Dokl.) USSR Acad. Sci.* **327**, 60–64.

Gryanik, V. M., Doronina, T. N., Olbers, D. J. & Warncke, T. H. 2000 The theory of three-dimensional hetons and vortex-dominated spreading in localized turbulent convection in a fast rotating stratified fluid. *J. Fluid Mech.* **423**, 71–125.

Gurulev, A. Y. & Kozlov, V. F. 1988 Numerical simulations of structure change on the potential vorticity fronts. *Izv. Atmos. Ocean. Phys.* **24**, 427–433.

Hogg, N. G. & Stommel, H. M. 1985 The heton, an elementary interaction between discrete baroclinic geostrophic vortices, and its implications concerning eddy heat-flow. *Proc. R. Soc. Lond.* A **397**, 1–20.

Ingersoll, A. P. 1990 Atmospheric dynamics of the outer planets. *Science* **248**, 976–979.

von Kármán, T. 1911 Über den Mechanismus des Widerstand den ein bewegter Körper in einer Flüssigkeit erfährt. *Nachrichten der K. Gesellschaft der Wissenschaften zu Göttingen Math.-phys. Klasse*, 1–9.

Kimball, J. & Hallinan, T. J. 1998 A morphological study of black vortex streets. *J. Geophys. Res.* **103** (A7), 14683–14695.

Korotaev, G. K. 1997 Radiating vortices in geophysical fluid dynamics. *Surveys Geophys.* **18**, 567–619.

Lamb, H. 1932 *Hydrodynamics*. Dover.

Legg, S. & Marshall, J. 1993 A heton model of the spreading stage of open-ocean deep convection. *J. Phys. Oceanogr.* **23**, 1040–1056.

Marcus, P. S. & Lee, C. 1998 A model for eastward and westward jets in laboratory experiments and planetary atmospheres. *Phys. Fluids* **9**, 1474–1488.

Masuda, A. & Miki, K. 1995 On the stability of baroclinic vortex streets composed of quasi-geostrophic point eddies. *Deep Sea Res.* **42**, 437–453.

Nycander, J. 1994 Steady vortices in plasmas and geophysical flows. *Chaos* **4**, 253–267.

Pao, H.-P., Lai, R. Y. & Schemm, C. E. 1982 Vortex trails in stratified fluids. *Johns Hopkins APL Technical Digest* **3**, 12–18.

Pedlosky, J. 1987 *Geophysical Fluid Dynamics*. Springer.

Poulin, F. J. & Flierl, G. R. 2003 The nonlinear evolution of barotropically unstable jets. *J. Phys. Oceanogr.* **33**, 2173–2192.

Pullin, D. I. & Saffman, P. G. 1998 Vortex dynamics in turbulence. *Annu. Rev. Fluid Mech.* **30**, 31–51.

Reznik, G. M. 1986 Point vortices on a β-plane and Rossby solitary waves. *Okeanologiya* **26**, 165–173.

Reznik, G. M. 1992 Dynamics of singular vortices on a beta-plane. *J. Fluid Mech.* **240**, 405–432.

Reznik, G. M., Grimshaw, R. H. J. & Sriskandarajah, K. 1997 On basic mechanisms governing two-layer vortices on a β-plane. *Geophys. Astrophys. Fluid Dyn.* **86**, 1–42.

Rintoul, S. R., Hughes, C. & Olbers, D. 2000 The antarctic circumpolar current system. In *Ocean Circulation and Climate* (ed. G. Siedler, J. Church & J. Gould) pp. 271–302. Academic.

Rosenhead, L. 1929 The Kármán street of vortices in a channel of finite breadth. *Phil. Trans. R. Soc. Lond.* **228**, 275–329.

Saffman, P. G. & Schatzman, J. C. 1981 Properties of a vortex street of finite vortices. *SIAM J. Sci. Statist Comput.* **2**, 285–295.

Saffman, P. G. & Schatzman, J. C. 1982 Stability of a vortex street of finite vortices. *J. Fluid Mech.* **117**, 171–185.

Shukla, P. K., Birk, G. T. & Bingham, R. 1985 Vortex streets driven by sheared flow and applications to black aurora. *J. Geophys. Res. Lett.* **22**, 671–674.

Sokolovskiy, M. A. & Verron, J. 2000 Finite-core hetons: stability and interactions. *J. Fluid Mech.* **423**, 127–154.

Sommeria, J., Meyers, D. & Swinney, H. L. 1991 Experiments on vortices and rossby waves in eastward and westward jets. In *Nonlinear Topics in Ocean Physics* (ed. A. R. Osborne) pp. 227–269. North-Holland.

Stenflo, L. 1994 Acoustic gravity vortex chains. *Phys. Lett.* A **186**, 133–134.

Stewart, H. J. 1945 Hydrodynamic problems arising from the investigation of the transverse circulation in the atmosphere. *Bull. Am. Math. Soc* **51**, 781–799.

Youssef, A. & Marcus, P. S. 2003 The dynamics of jovian white ovals from formation to merger. *Icarus* **162**, 74–93.

Wolff, J.-O., Maier-Reimer, E. & Olbers, D. J. 1991 Wind-driven flow over topography in a zonal β-plane channel: A quasi-geostrophic model of the antarctic circumpolar current. *J. Phys. Oceanogr* **21**, 236–265.